ADDIS ABABA UNIVERSITY

ADDIS ABABA INSTITUTE OF TECHNOLOGY

SCHOOL OF MECHANICAL AND INDUSTRIAL ENGINEERING

Analysis of Rolling Contact Fatigue Damage and Fatigue Life Comparison of Rail Due to Cyclic Axle Load

By

Ayana Gebremichael

A Thesis Submitted To the Graduate School of Addis Ababa University in Partial Fulfillment of the Requirements for the Degree of Masters of Science

Master of Science

In

Mechanical Engineering

(Under Railway Engineering)

Advisor

Dr. Daniel Tilahun

September, 2014

ADDIS ABABA UNIVERSITY

ADDIS ABABA INSTITUTE OF TECHNOLOGY

SCHOOL OF MECHANICAL AND INDUSTRIAL ENGINEERING

Analysis of Rolling Contact Fatigue Damage and Fatigue Life Comparison of Rail Due to Cyclic Axle Load

By

Ayana Gebremichael

September, 2014

Approved by Board of Examining:

Birhanu Beshah (Dr.)	_____	_____
Head, Railway center	Signature	Dat
Daniel Tilahun (Dr.)	_____	_____
Advisor	Signature	Date
Ato Tollossa Dreibsa (MSc)	_____	_____
Internal Examiner	Signature	Date
Ato Tsegaye Feleke (MSc)	_____	_____
External Examiner	Signature	Date

ACKNOWLEDGEMENT

First of all, enormous thanks to almighty God for his priceless help to finish my thesis successfully.

I would like to thank my advisor Dr. Daniel Tilahun for making this work possible. I am very grateful for his guidance, support and encouragement throughout this research. Also co- advisors, Ato Habtamu Lekubet and Ato Mulugeta for their follow up and supervisions.

I would like to thank Ato Endalkachew from Addis Ababa University who is workshop and laboratory superintendant and helped me by giving the necessary advice and support for the possible outcomes from the test I was conducting.

Also thanks to Engineer Behailu Sentayhu from Ethiopian Railway Corporation LRT Project Manager for his positive cooperation and providing me material for the test and all the required data's.

Finally, I would like to thank everyone who supports me in my entire period of study.

ABSTRACT

This paper presents the analysis of rolling contact fatigue damage due to cyclic axle load between wheel/rail and fatigue life comparison between experimental and ANSYS results. The purpose is to see the fatigue life of the rail and to protect it from failure. .For this analysis a three-dimensional finite element model of the wheel/rail interaction is used to investigate the effect of the applied contact loading force at the straight area of the wheel tread and railhead surface. For the experimental part, fatigue test is conducted by taking specimens from the rail material and the specimens are modeled by CATIA V5 and analysis the effect with ANSYS 12.0 by applying different loads for the comparison of the fatigue life. Throughout the whole analysis, the Hertz contact theory assumptions are basically considered. Form the wheel/rail fatigue life analysis the result found is see the maximum life found by the applied load. The specimen numerical and experimental result shows that the experimental analysis is more preferable and precise. The application of this study is to identify and protect the rail from failure and to insure safety of the passengers and minimize maintenance cost.

Keywords: Rolling contact fatigue failure, Cyclic load, Rail Fatigue life.

Contents

LIST OF TABLES

LIST OF FIGURES

NOMENCLATURES

UIC: International union of railways

RCF: Rolling Contact Fatigue

HCT: Hertz's Contact Theory

N_f: Number of Load Cycles to Failure

N_i: Crack Initiation Life

N_g: Crack Growth or Propagation Life

LEFM: Linear Elastic Fracture Mechanics

ΔK: Intensity Factor

da_o/dN: Crack Growth rate

AA LRT: Addis Ababa light rail transit

σ_a : Applied Stress

σ_{UTS}: Ultimate Tensile Strength of Rail

b: Material Specific Fatigue Parameters

S_e : Endurance Limit

R_1^w: The Principal Rolling Radii of the Wheel

R_2^w: The principal transverse radii of the wheel

R_1^r: The principal rolling radii of the rail

R_2^r: The principal transverse radii of the rail

Z: Contact Point Depth

a: Major Semi-axis

b: Minor Semi-axis

$d(x,y)$: Vertical Relative Distance

P: Contact Pressure

P_o: Maximum Contact Pressure

F_n: The Applied Normal Load at the Wheel/rail Contact

K_w: Constants that depend on the material properties of wheel.

K_r: Constants that depend on the material properties of rail.

K_3: Geometrical Properties of both Wheel and Rail.

v^w and E^w: Poisson's ratio and Young's Modulus of the railway Wheel Material

v^r and E^r: Poisson's ratio and Young's Modulus of railway Rail Material.

M and n: Hertz coefficients

φ: Yaw Rotation Angle (The angle of the orientation difference of the principle axes of the two bodies)

ω: Angular Velocity of the Wheel

v: Maximum Operation Speed of the Vehicle

SF-1: Load applied on fatigue testing unit machine

SV-1: Motor speed of the fatigue testing unit machine

CHAPTER ONE: INTRODUCTION

1.1. Background of the Research

The history of rail transport starts nearly at 600 BC systems with man or horse power, and tracks or guides made of stone or wood in ancient Rome and Greece. Wagon ways (or 'tramways') are thought to have developed in Germany in the 1550s to facilitate the transport of ore tubs to and from mines, utilizing primitive wooden rails. The first railway was completed in 1604 in British. Mechanized rail transport systems first appeared in England on 1820s. These systems, which made use of the steam locomotive, were critical to the Industrial revolution and to the development of export economies across the world. They have remained the primary form of land transport ever since for most of the world. Because a stiff wheel rolling on a rigid rail requires less energy per ton-mile moved than road transport, railroads are highly suitable for the movement of dense, bulk goods such as coal and other minerals. This was an encouragement to focus a great deal of inventiveness upon the possible configurations and shapes of wheels and rails. In the late 1760s, fixing plates of cast iron to the upper surface of the wooden rails began. The improvements and innovations are continued and the first full scale working railway steam locomotive was built in the United Kingdom in 1804.The introduction of Bessemer process, enabling high quality steel to be made inexpensively, led to use steel rails at first in Britain 1857.In 1900, the railway was mostly completed, and there were more than a hundred train companies in Great Britain. In 1904, an engine called 'The City of Truro' became the first to travel at more than 100 miles an hour. The electrification of the railways began in 1933. This means that the trains began to run on electricity instead of steam. Railways were originally intended to carry mostly goods rather than passengers but in the 1970s, the value of carrying passengers overtook goods for the first time [3].

The railway lines construction in Ethiopia was first started in October 1897 from Ethiopia to the port of Djibouti in the regime of Emperor Menelek II. The first commercial service began in July 1901, from Djibouti to Dire Dawa. By 1915 the line reached Akaki, only 23 kilometers from the capital, and two years later came all the way to Addis Ababa itself

[4]. Transportation infrastructure in Ethiopia has been neglected for decades, but is now a priority of the government of Ethiopia and the new network rail transport is under construction.

The railway transport system is one of the most crucial transport systems in the world with mass transport, very high speed, safety and durability. Now a day, there is a high demand of railway transportation systems in the world including in Ethiopia for a short and long distance transport of passengers and goods. The new rail network in Ethiopia and the railway track must show the necessity of an efficient management of railway systems. The design must aim toward reducing costs and increasing safety, as well as reliability of the railway systems. The wheel/rail interface is one of the most crucial points that must be checked to determine the performance of a train and consider its safety. However, the calculation of the stress at the wheel/rail interface is dependent on the static and dynamic loading. The damage in this area is due to train speed, type of rolling stock, cyclic axle loads, track lay-out and track geometry parameters, rail material properties, temperature or humidity [2]. The damages that affect the mechanisms of fatigue are some of the concerns for the life prediction for a railway track. Fatigue causes abrupt fractures in the railhead and wheel tread. These failures may cause damage to rails because of the stress caused by the contact force. This paper presents the analysis of rolling contact fatigue damage due to cyclic axle load on the rail and fatigue life for the light rail transit (LRT) in Ethiopia. Also by taking specimen from the rail and conduct experimental fatigue test and compare it with ANSYS simulation.

After having a built up of trains with a relevant rail track systems, there is a periodic maintenance schedule. Due to the applications of different load cycles, relative rolling sliding motion of wheels on rail tracks, inappropriate geometrical fitness of wheel/rail contact profile and some other factors the maintenance schedule mainly concerns about the wheel/rail interaction systems. To reduce such maintenance costs it is better to analyze and understand the wheel/rail contact behavior and applied load conditions. The analysis of wheel/rail contact requires the detail analysis of the contacting surface conditions and factors affecting the contacting surface behavior of the two machine components (rail-wheel). Therefore to understand the general functions and properties of

the two machine components (wheel/rail), it is preferable to see the sub components as follows.

1.1.1. Railway Track

Railway truck is laid on the appropriate ground level and geographical sites based on the appropriate design specification. It has different components interrelated with meaningful arrangements for the general railway dynamic operations. Rail track is a fundamental part of railway infrastructure and its components can be classified into two main categories: superstructure and substructure. The most obvious parts of the track as the rails, rail pads, sleepers, and fastening systems are referred to as the superstructure while the substructure is associated with a geotechnical system consisting of ballast, sub-ballast and sub grade (formation). Both superstructure and substructure are mutually important in ensuring the safety and comfort of passengers and quality of the ride. The typical shape and construction profiles of a ballasted track are illustrated in figure 1.1.

The rail track sleeper is used to transmit the wheel load to the ballast medium. In addition, it has functions such as maintaining track alignment and gauge, restraining longitudinal and lateral rail movements, and providing strength and stability to track structure [11]. The rail joints are used to join rails depending on the required position.

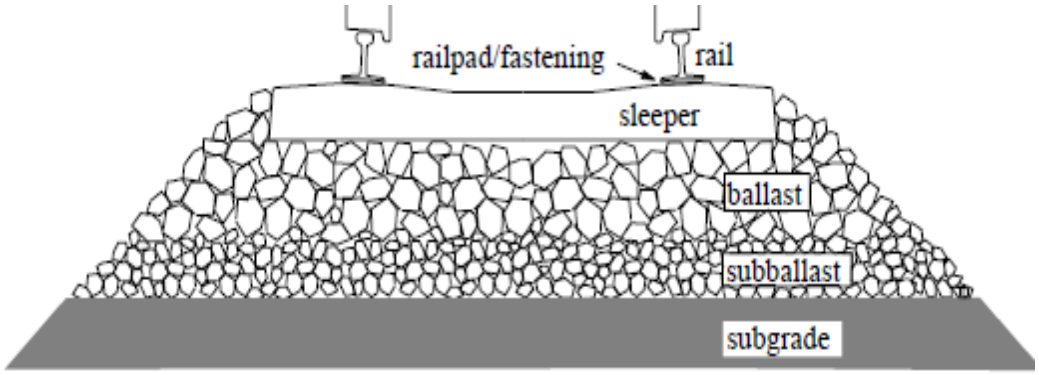

Figure 1.1: Rail track components and their arrangements

During the interaction between the wheel set and the rail track there are different conditions created on the contacting surface. These dynamic contact behaviors depend partly on the track geometry. The most common track geometries having great impact on the railway vehicle dynamic behavior are track gauge (the distance between the right and

left rail inner gauge corners), track cant (the difference between the level of the two rail on a curve), track curvature (it is the inverse of the radius of the curved track), rail head (it is the surface of the rail having a direct contact to the railway vehicle wheel set) and wheel and rail tread profile.

By managing those geometrical parameters of the track it is possible to control the dynamic behaviors of the wheel-rail dynamic contact, especially on the curved track.

1.1.2. Rail-Wheel Interaction

Rails play a significant role in transport of passengers and fright movements. Increasing traffic density, axle loads, accumulated tonnage, train speed and longer trains have increased productivity but with an increased risk of break and derailments. Rail wear and rolling contact fatigue (RCF) are inevitable due to wheel/rail interaction. These problems have increased the maintenance and replacement costs. If undetected, these problems can cause derailment causing huge loss of revenue, disruption of service, resulting damage of assets, and loss of lives. Rolling contact fatigue (RCF) alone costs huge amount of money per year and these defects account high percent of the total costs. The office for research and Experiments (ORE) of the International Union of Railways (UIC) has noted that maintenance costs increases directly (60-65 percent) with increase in traffic, train speed and axle load. These costs are greater when the quality of the track is poor [12].

In rail transportation, operational risks are defined as risks of rail breaks and derailments that occur during the rail-wheel interaction. During the rail-wheel interaction, some of these unwanted events occur due to lack of maintenance, rail-wheel wear and rolling contact fatigue (RCF) cracks. These are influenced by various operating conditions such as traffic density, fright, rail material type, size, hardness, bogie type, speed limit, temperature, curve radius and environmental factors. Risks have been increasing due to increased number of axle passes, steeper curve radius, worn-out-rail-wheel profile in the system and inappropriate rail-wheel grinding, poor lubrication and poor maintenance. Modeling and analysis of operating risks require failure time date, probability of detection and consequences of failures. Interpretation of various rail defects and broken rails and their consequences is extremely important for developing these models.

Preventive rail grinding and lubrication is used to control surface fatigue detects and to reduce wear and noise. However, knowledge of surface fatigue cracks, rail-wheel wear, rail grinding and lubrication is limited.

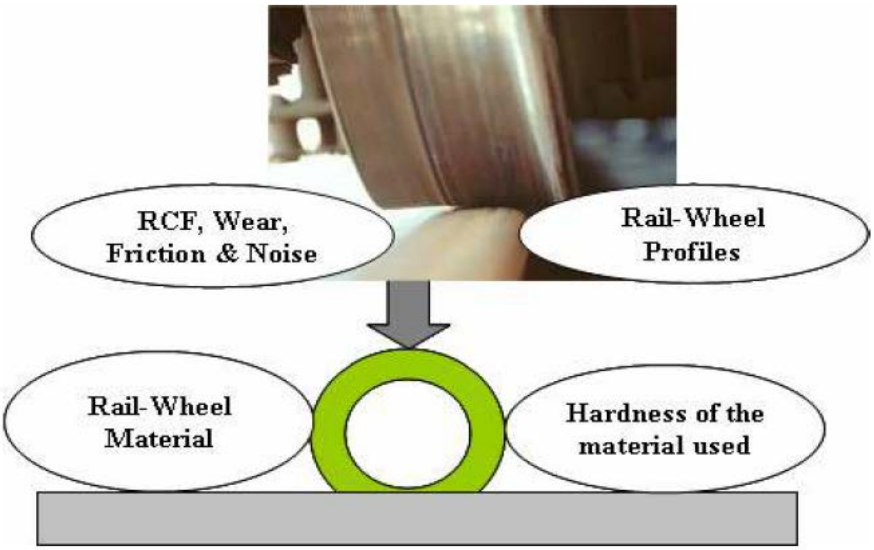

Figure 1.2: Factors behind the problem

Some of the factors behind the problems are in Figure 1.4. It is important to study the interaction of wheel/rail degradation and influencing factors, monitor those factors and find cost effective technological solutions to eliminate or reduce those problems. Therefore, there is a need to develop an integrated model to predict operational risks, and take appropriate economic decision to reduce maintenance cost and improve reliability and safety of rail operation.

Understanding of interaction between wheel and rail indicates and predicts the way how to treat them and how to prevent them from failures which is a better guide to select the appropriate materials, geometry, design, orientation etc. That is why this paper mainly concerns about the analysis of wheel rail rolling contact and applied load condition on the rail head surface.

1.1.3. Rolling contact Fatigue (RCF)

Fatigue began to be recognized as a specific failure mode when the early railways began to suffer failures of axles, wheels, rails, boilers and other components [10]. Much impetus

for investigations into fatigue stemmed from the first railway accident to cause a major death toll, which occurred near Versailles in 1842 [14] when the axle of a locomotive broke. During the next two decades, the great German railway engineer Wöhler, demonstrated that cyclic stress ranges determined fatigue lives and that for steels at least, a fatigue limiting stress existed, below which fatigue lives were infinite. The S/N curve, relating stress range to cycles to failure and the fatigue limit, still remain the basis of design against classical fatigue. The mechanism of fatigue has been unraveled during the 20th century, particularly in the last fifty years. It is now known that fatigue is caused by the initiation and growth of cracks.

Rolling contact fatigue (RCF) is a family of damage phenomena that appear on and in rails due to over stressing of the rail material. This damage may appear first on the surface or the subsurface. In either case, these phenomena are the result of repeated over stressing of the surface or subsurface material by the hundreds or thousands or millions of intense wheel/rail contact cycles.

According to [5], the problem of RCF in rails grew in size both domestically and internationally through the 1990s, and was brought to worldwide attention through the loss of life in the Hatfield (UK) derailment in 2000. Beyond the safety implications, there is a substantial economic cost associated with RCF. In 1999 [13] a European study suggests that the cost of RCF to the European railway network, including inspection, train delay, rail replacements and weld repair, rail grinding and derailments, is about 300 million € per year. The cost of RCF to the North American rail industry is believed to be a significantly greater amount.

Two key processes govern RCF are crack initiation and crack propagation. These processes are governed by a number of factors including environmental conditions, rail and wheel profiles, track curvatures, grades, lubrication practices, rail metallurgy, vehicle characteristics, track geometry errors, and rail grinding practices. They all play a role in the formation of RCF and inversely can be used to control and minimize RCF.

The amplitude and position of the crack initiating stresses varies depending on the contact geometry, load, and friction conditions. Under high friction conditions shear stresses are large but very shallow. Under low friction conditions, the peak shear stress

decreases but extends deeper into the railhead. The result is that some RCF defects are initiated at the surface and others below the surface.

1.1.4. Types of RCF Defects

Rolling contact fatigue will lead to surface and subsurface cracks as stated earlier. Based on the nature and location of the failures, they are classified as follows [7].

I. Surface Initiated Defects

Head Checks: develop on outer rail of the shallow curves in the form of a series of cracks as shown in Fig. 1.3 and present the biggest problem in rails. These can also develop on sharp curves having limited or no wear. They result from accumulation of plastic strain increments, which eventually exhausts the ductility of the surface material, at which point cracks can initiate. The critical conditions for this to occur are high load and friction.
These head checks have been found extensively on straight track also due to hunting. Bad weld geometry and closely conformal rail/wheel contacts have been the cause of extensive hunting on straight track.

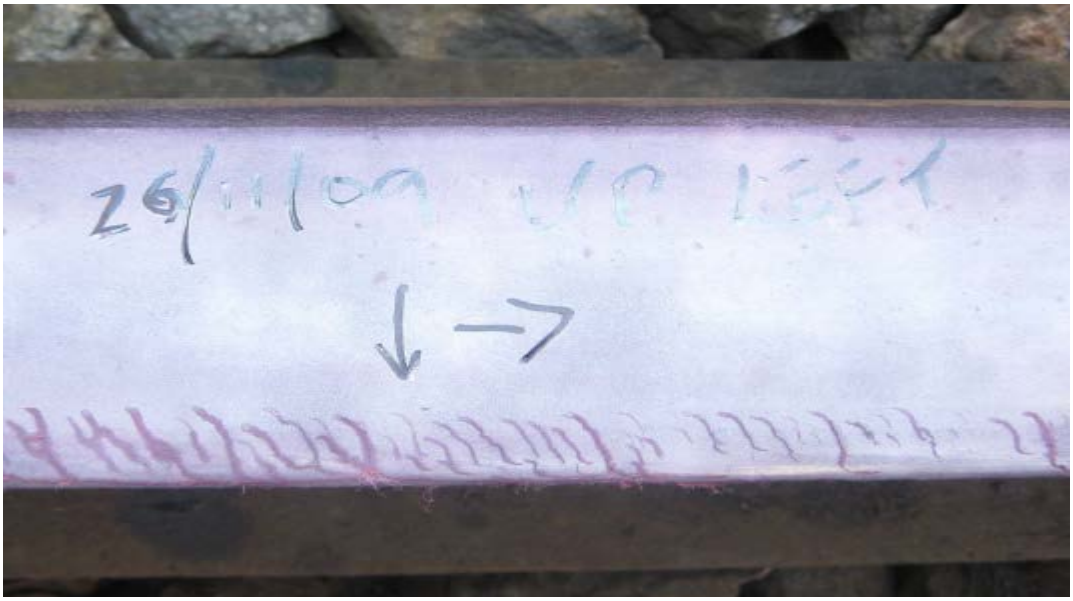

Figure 1.3: Head checks in rail

The head checks will grow with passage of traffic and their pitch will also reduce. The cracks not only grow on the surface but also penetrate deeper into the rail. It is, therefore, necessary to eliminate these head checks at the initial stages of their development.

Squats: occur on tangent track and in shallow curves on the rolling surface of the rail head and are characterized by dark spots on the rail as shown in Fig. 1.4.Squats are surface initiated rolling contact fatigue defects and may propagate transversely across the rail. They can initiate as a result of ratcheting and fluid pressurization and also from white etching layers which result from modification of the microstructure of the rail surface material from perlite to martensite. Ultrasonic inspection of these defects is difficult since the transverse defect is shielded by the shallow horizontal crack.

Figure 1.4: Squats in Rail

Spalling: occurs in the form of chipping off of metal from the rail gauge corner or from surface of the rail. The uncontrolled growth of head checks brings them closer resulting in joining of the cracks and material flakes coming out of the rail head. These may grow in transverse flaw with the passage of the traffic, endangering the integrity of the rail.

II. Sub-Surface Initiated Cracks

Shelling: Shelling and Spalling are similar type of defects, the difference being in their initiation. Spalling is a surface phenomenon, while shelling is a sub-surface initiated defect. The crack starts developing below the rail surface due to inclusions coupled with heavy stresses. The crack grows towards the head and chipping-off of the material occurs.

Gauge Corner Defects: These effects are formed on the high rails in curves of sharper radius generally and on routes of heavy axle loads with moderate speeds.

An elliptical shell-like crack with characteristic crack growth rings propagating transverse to rail section under the influence of contact stresses and shear stress develops at first. Later due to bulk stresses and residual stresses in the rails, cracks initiate from the shell either upward or downward. The upward cracks lead to shelling on the Gauge face, where as downward propagation will lead to fracture/formation of kidney.

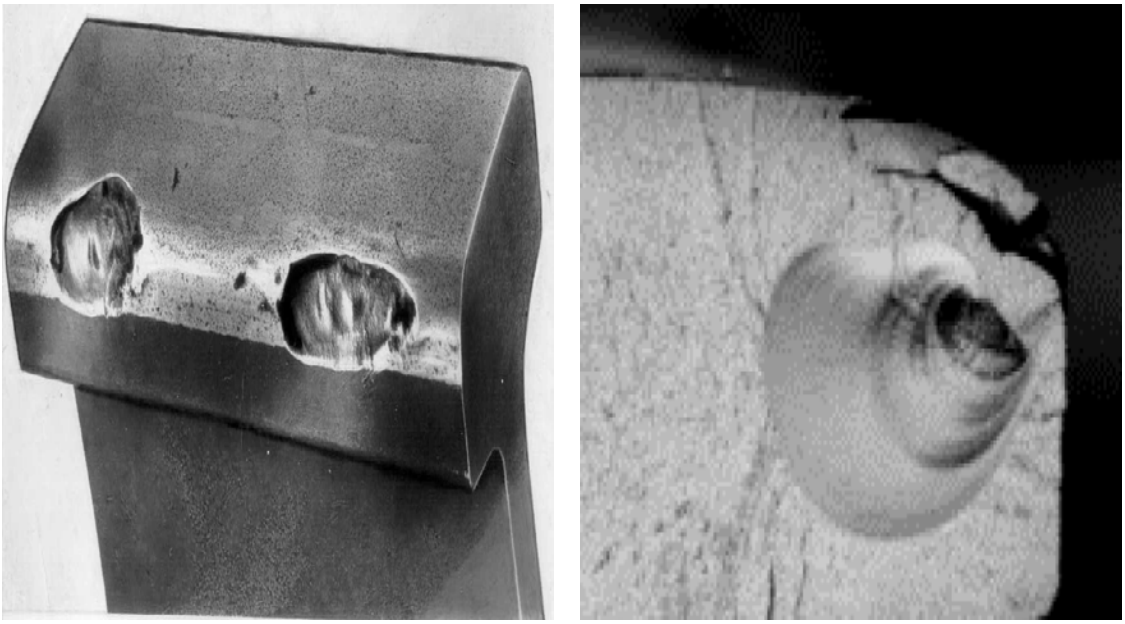

a) Upward Cracks b) Downward Cracks

Figure 1.5: Gauge Corner Defects in Rail

1.2. Statement of the Problem

Rolling contact fatigue failure analysis is used to analyze the cause, type and position of failures. However, these are depends on the standard materials, operating conditions and wheels and rails under consideration. Depending on the cause, type and position of the rolling contact fatigue, the way of distribution of cyclic axle load and its effects differs accordingly. The effects due to this cyclic load are damage (crack) initiation, propagation and failure. Fatigue life analysis is helping to identify this failure and take measure. In this study the fatigue life of the rail is compared between ANSYS simulation and

experimental test. In the new network rail transport in Ethiopia if these problems are not analyzed from the start and ignored, it will cost more in incidents, accidents, fatality and excess maintenance cost. RCF analysis will help to minimize rail maintenance, improve safety and life-cycle matters.

1.3. Objective of the Research

1.3.1. General Objective

The major objective of this paper is to analyze the rolling contact fatigue failure and comparison of fatigue life of the rail by experimental and numerical methods due to cyclic axle load.

1.3.2. Specific Objective

- Develop 3D modeling of wheel and rail using CATIA V5 software.
- Determine fatigue life of the rail by analyzing with ANSYS 12.0 software.
- Machined 4 specimens from specified position of the rail
- Conduct fatigue experiment to see the fatigue life with different loading condition.
- Model the specimen with ANSYS 12.0 and analyze it.
- Compare it the fatigue life found from ANSYS 12.0 and the experiment result.

1.4. Scope and Limitations of the Research

As it is seen in the problem statement there are many problems that affect the analysis of rolling contact fatigue and fatigue life of rail and this study mainly focuses on the fatigue failure caused by cyclic axle load on the rail and the fatigue life for Addis Ababa light rail transit.

1.4.1. Scope of Finite Element Modeling

Predicting fatigue life of the rail is the main scope of the finite element study for wheel/rail analysis and comparison of fatigue life for the specimen by experimental and finite element method, taking into consideration different loading. Rail life prediction is based on the RCF failure mechanisms, although wear and RCF mechanisms cannot be

separated in real rail networks, the majority of catastrophic failures are a result of cracks initiated due to RCF.

Due to the complexity of the modeling, unlicensed ANSYS software and time limitation factors, the following aspects are considered to be outside of scope of this research.

- Prediction of crack initiation at the rail.
- Crack propagation.
- Curved and transition track scenario.
- Lubrication and friction effect.

1.4.2. Scope of the Experimental Study

The scope of the experimental study is to identify the fatigue life of the rail by the specimen taken from it. Main limitations of the test specimen used are the inability of the leath machine and skill or precision of the persons who prepare it, which limits the experimental simulations. As a result, the cycles of failure of the specimens are fast and it is difficult to find the proper output.

1.5. Thesis Outline

This thesis contains five chapters presenting the research findings. The content of each chapter is briefly outlined in what follows:

Chapter one outlines general information about the research conducted. Initially, the basis behind the research are discussed and presented. This is followed by the general and specific objectives of this research to minimize the identified gaps. After that, the scope and the limitations of this research are pointed out. Finally, the thesis structure is presented by summarizing all of the chapters.

Chapter two reviews published research relevant to the thesis topic. The cause and the methods for analysis of crack initiation, crack propagation is reviewed. Also the analysis of RCF failure and prediction of fatigue life of the rail is seen.

Experimental/Analytical methods and conditions are described in chapter three. The material type used for the analysis, conditions of operation and experimental apparatus and procedures are discussed. This chapter also describes the dimensions of the

specimens for the fatigue test and procedures of the experiment. Additionally, the FE analysis by ANSYS 12.0 software is modeled.

Chapter four describes the results found by ANSYS 12.0 for wheel/rail and the specimen analyzed by this software. Also the result from the experimental tests carried out in the specimen for fatigue life and discussed the results by comparing with ANSYS 12.0 result.

The main findings of the study are summarized in chapter five along with recommendations for application. Also the improvement or/and related studies are suggested for future work.

CHAPTER TWO: LITERATURE REVIEW

2.1. Introduction

Review of literatures reveals that different previous work which helps for the guidance of this work. These previous related works may be journals, conference papers, design works and books related to this paper. Selection of appropriate conditions, approaches and methodologies with these journals and other materials will strengthen for the successful accomplishment of the paper

2.2. Rail rolling Contact Fatigue

Rolling Contact Fatigue (RCF) in rails was known in the late 1990s but was underestimated [6]. Now, with the high speed, dense traffic and high axle loads of modern railways, RCF has become a more serious problem highlighted by the Hatfield train disaster. Factors affecting RCF are rail curve radius, wheel base, wheel diameter, axle load, primary yaw stiffness of suspension, rail-wheel profiles, traction, braking forces and wheel/rail material property. RCF is traditionally known (and recognized) by its surface manifestations and was widely known as ‘squat’ in Britain and in Japan as ‘black spot’.

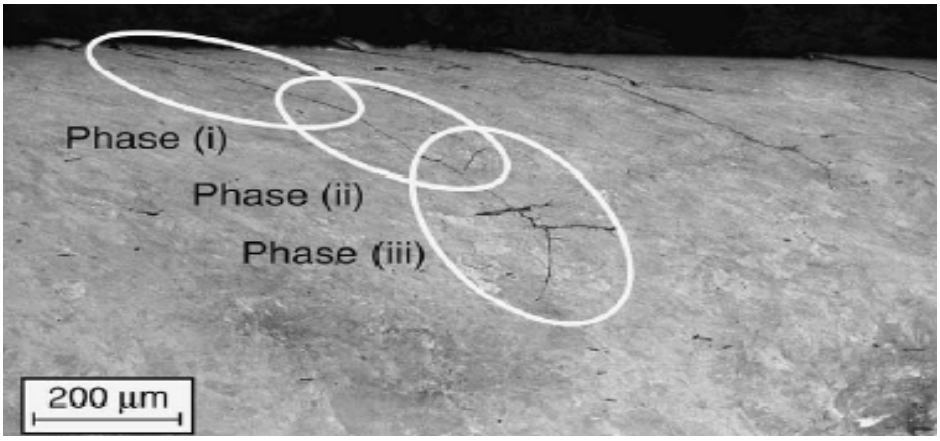

Figure 2.1: Three phases at the surface

RCF is associated with plastic deformation under contact forces and a crack initiates (Figure 2.1) due to a unidirectional accumulation of strain that propagates downward

under successive applications of compressive contact stresses. Oliver [15] explains that, if the contacting bodies are smooth, loaded below the elastic limit and not subjected to any tractive forces, then the stress field near the contact is just that due to the Hertz pressure distribution. This may also even be true if the contacting surfaces are not perfectly smooth but are lubricated with oil giving a film thickness that is large compared to the roughness of the contacting surfaces. Load passing gives a two dimensional profile with shear stress varying with depth and compressive direct stress varying with width. These stresses are not proportional to time so, in this respect, even the simplest RCF differs from classical fatigue. The situation is more complex in realistic conditions where roughness is appreciable and tractive or sliding forces are involved, so during RCF, the stresses are local, compressive, non-proportional to time and randomly fluctuating indirection and magnitude. Plastic deformation often precedes crack formation on the scale of either the Hertz contact or the roughness. This happens under elastic and plastic shakedown loads (Figure 2.2). In hard materials, RCF is less commonly accompanied with plasticity. Here, crack initiation occurs at surface asperities, dents or subsurface inclusions.

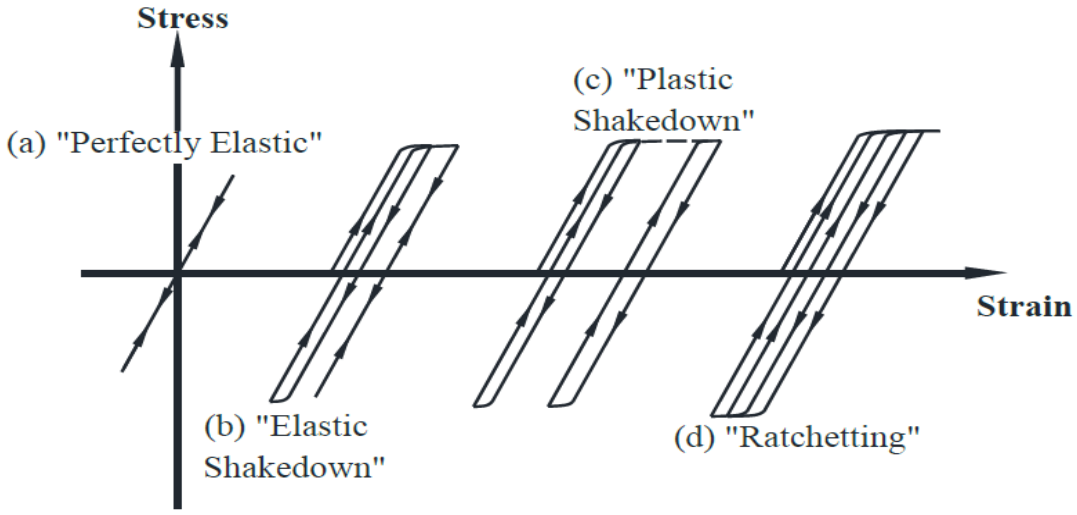

Figure 2.2: Material response to cyclic loading

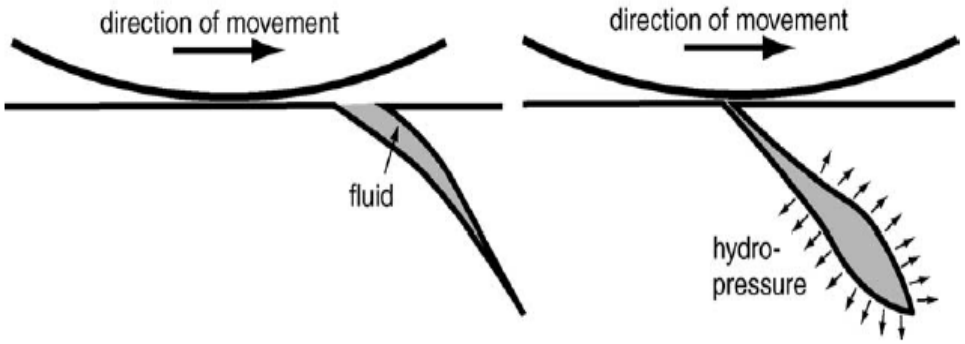

Figure 2.3: Crack propagation mechanism by pressure of trapped fluid

Further, due to stain localization, compressive stresses become extensive at crack closure and RCF develops due to crack face friction and interlocking that initially causes crack development, which is mechanically influenced by lubrication near the crack face (Figure2.3). Microstructure changes occur in the locality of the crack origin due to stain localization and secondary damage arises from fretting. RCF also gives rise to spherical debris particles from the relative tangential displacement of crack surfaces. Finally RCF changes the topography of the contacting surfaces which, in turn, affects the contact pressure and hence contact stresses that drive the fatigue mechanism. This paper is not included the effect of surface roughness and sliding force effect for the RCF crack initiation.

The crack extends downward from its origin near the surface and the direction of downward crack propagation depends upon the traction forces and is usually at about 20° to the surface. Stable growth of the inclined crack seems to be controlled by the direction of the motion of the controlled zone rather than the traction force. Linear elastic fracture mechanics (LEFM) studies suggest shear crack propagation driven by contact stress (Mode II and Mode III), entrapment of fluid in high pressure contacts leading to opening (Mode I), crack mouth closure trapping the fluid in the crack with contact motion generated fluid pressure at the crack tip (Mode I). The direction of crack propagation from its initiation is crucial in determining the significance of the problem and the growth rate and direction reflects the direction of the prevailing tangential forces. Fluid (e.g. water or lubricant) entrapment [16] (Figure 2.3) will pressurize the crack tip under compressive load and add to the rate of crack propagation. Chue [17] have identified

strain hardening as an additional governing factor in pit formation under RCF over the traditional factors (initial crack length, crack angle, contact force, friction, and hydraulic pressure of trapped fluid). The twin disc test [18] is use routinely to study RCF. Crack initiation and propagation is induced by repetitive rolling and sliding between two mating surfaces. Fatigue crack propagation in mode I has been studied by Ringsberg [18], Olver [15]and many other authors with the consistent conclusion that crack initiation is due to shear stress at the surface, but mixed mode cracking is still proving difficult to understand. The simplest RCF effect occurs in straight tracks or with gentle curves and manifests itself as squats. Squats occur under normal loading and are cracks, 25 to 50mmin length, which initiate below the surface and propagate at a shallow angle to the surface before branching upwards to form a spall or downwards, which can cause catastrophic failure. Squat formation and propagation only require rolling contact, but their propagation rate may be aggravated by pressure due to trapped fluid [19], traction forces and/or shear between rail and wheel or by the presence of a white etching layer or an object on the rail surface. Ringsberg focused only on the trapped fluid crack propagation.

The length of the initial shear crack depends upon the stress intensity exposure [20]. The range in stress intensity factor, ΔK, is known to be the driver for crack growth rate, da_o/dN, through the Paris equation, $\frac{da_o}{dN} = n\Delta K^m$ where, n, m are experimentally obtained constants, N is the number of fatigue cycles and a_0 is crack depth. Li [22] studied short vertical crack formation in RCF of a medium carbon, bainitic back up roller under conditions of low contact pressure and pure rolling. Vertical short crack initiation and propagation were tracked by microscopic observation. They found that vertical short cracks form at the initial stage of rolling contact fatigue in the direction parallel to the axis of the upper roller due to tensile stress. These short cracks stopped propagating between 10^4 and $3\text{-}5\times10^5$ cycles (70% to 80% of the surface distress life) because of the decreasing stress with depth in the roller contact zone. Towards the end of life they start propagating again at a higher rate in a circumferential direction and parallel to the contact surface due to severe ratcheting at the tip of the crack caused by shear stresses.

Farris [23] found a reasonable correlation between calculated and experimental rates of shell crack growth, horizontal rail cracks located about 6-7mm below the surface of the rail. The shells are generally considered to be benign as they are not associated directly with rail failure, although they may grow out of the horizontal plane and cause vertical detail fractures that can lead to rail failure. Here, the leading edge of a short shell grows out of plane and initiates detail fracture in unidirectional train traffic. However, the trailing edge is branching up towards the surface and, when the train traffic is reversed, the leading edge becomes the trailing edge so a wavy crack path arises due to out of plane growth. Kim [24] studied the shelling to transverse crack growth rates in rail under Mode I and mixed mode and concluded that, under mixed mode, fatigue crack growth rate is slower than mode I, and the difference decreases with increasing stress ratio.

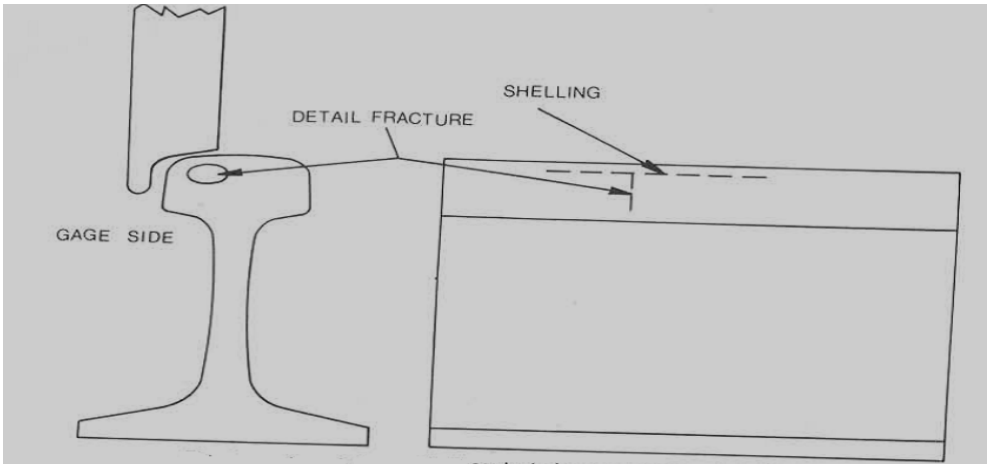

Figure 2.4: Schematic of wheel/rail contact showing shelling and detail fracture

Jeong and Orringer [25] predicted surface crack growth in rail webs (Figure 2.4) using FEM and elementary beam analysis. Both models were based on different assumptions but the calculated crack growth rate was found to be very slow in both cases allowing detection long before failure. Olofsson and Nilsson [26] have studied crack initiation and propagation with and without lubrication in two different rail steel grades (UIC900 A of UTS900N/mm2 and UIC1100 A steel of UTS 1100N/mm2) over two years in real rails with curve radii of 300mm and 600mm. Both materials seemed to be similarly sensitive to crack initiation but the 1100 grade rail was more sensitive to crack propagation and also more sensitive to head-checks, showing signs after 1 month of traffic as opposed to

two years for the 900 grade. As expected, lubrication reduced the amount of profile change and also reduced the crack propagation rate, which was less expected. They explained this by the reduction of coefficient of friction, leading to lower tangential stresses in the contact zone between wheel and rail. Sensitivity to crack initiation on lubricated 1100 grade rail was still the same but the crack length and wear rate were reduced.

N.A. Akeel, Z. Sajuri and A.K. Ariffin [21] studies damage on the rail head surface and wheel tread due to rolling contact fatigue. This paper analysis RCF damage initiation and stress distribution at the wheel/rail interface at different directions. A three-dimensional elastic frictional finite element model of the wheel/rail interaction is used to investigate the effect of the applied contact loading force at the straight, transition, and curved areas of the wheel tread and railhead surface. The interface exhibits small damage problems that are solved via the finite element method (FEM) software code ANSYS 11. The half-space assumption of the Hertz method is avoided by FEM. The result indicates stress decreases at the straight area in the wheel-rail contact model compared with those at the transition and curved areas of the rail track. The effect of fatigue damage life initiation increases at the straight area but decreases at the transition and curved areas in the wheel/rail contact model and the maximum value of fatigue life prediction at the straight area.

In Ethiopia, there is a shallow or few researches have been done on railway area. Specifically, when we come to rolling contact fatigue failure due to cyclic load at wheel/rail interface, there is a huge gap of conducted research in the area. Therefore this study is expected to give a start to fill this gap in this area.

Finally, in this paper, we are identifying the fatigue life of the rail both in ANSYS 12.0 and fatigue testing method and compare the results. The main issues here are safety, comfort and minimize cost of maintenance. As a transport giving sector, Ethiopia Railway Corporation (ERC) must give priority to this problem from the start of the network project. By this the service which we get from it and the development of the country will be continuous as planned.

CHAPTER THREE:

EXPERIMENTAL/ANALYTICAL METHODS AND CONDITIONS

3.1. Wheel/Rail Material

Around the world, there are various manufacturers of wheel and rail materials. Wheel and rail materials are quite similar in composition, differing slightly in the amounts of carbon, silica, and manganese in the steels used. It is widely known in tribology that pairs of similar metals can exhibit high adhesion and should generally be avoided in applications where they come into contact with each other [27], so changing one of these materials might reduce wheel and rail wear. However, there are other damage mechanisms to consider except wear when discussing the material properties, for example rolling contact fatigue and corrugation. Wear resistance is considered one of the most important characteristics of a rail steel. Pearlitic steel is the most widely used such steel, as the pearlitic microstructure resists wear and rolling contact fatigue [28]. Another important feature of wheel and rail materials is inclusions, which may cause cracking and high wear rates. In other types of materials, such as the nodular cast iron, carbon nodules are naturally embedded in the material. Railway wheels made of austempered ductile iron (ADI) containing graphite nodules were studied by Kuna et al. [29] and Mädler [30], who found that this material combines the advantages of high wear resistance and high fatigue strength with the wear-reducing side effect of the graphite inclusions, which act as lubricants on the contact surfaces. The main disadvantage of austempered ductile iron is that its fracture toughness is lower than that of the steels regularly used in the wheel–rail contact. In some contexts, ductile iron is also called nodular cast iron. Mädler [35] reports that ADI has been used by the Finnish National Rail System for railway wheels. Its use reduced life-cycle costs, but also resulted in some wheel tread failures [31].

Using measurements made in the field and the experimental results of pin-on-disc and twin-disc testing, Lewis and Olofsson [28] found that the introduction of more modern rail materials has reduced the wear rate by up to an order of magnitude over the last 20

years. This finding highlights the importance of high-performance wheel and rail steels. Coatings have been demonstrated to have a positive effect on product longevity under severe conditions. Ringsberg [33] conducted theoretical, laboratory, and field studies of surface coatings on rails in highly loaded wheel/rail contacts and found reductions in rolling contact fatigue (RCF) damage and wear.

Rails are grouped according to their standards, strength, grade, quality and length. The rail steel qualities can be distinguished in to two categories.

- ✓ Normal steel quality with an ultimate tensile strength of 700-900 MPa.
- ✓ Hard steel quality used mainly on curves, and crossings etc. with an ultimate tensile strength of 900-1200 MPa.

Concerning their chemical compositions rails have great varieties of carbon, manganese, chromium and silicon contents depending on their requirements. Since the rails have to withstand the impact load, friction and stress of freights, they should have sufficient strength, hardness, toughness and good welding performance. However a large increase in rail mechanical strength may result brittle failure and as a result a further increase is not desirable. Similarly, the same material property is selected for wheel materials.

For Addis Ababa light rail transit (AA LRT), the rail standard used is China National Railways standard of 50 kg/m. Wheel and rail materials are quite similar in composition, differing slightly in the amounts of chemical composition in the steels used. Table 3.1 presents the chemical compositions and table 3.2 shows mechanical property of rail material.

Table 3.1: The chemical compositions of the rail material.

Material	C (%)	Si (%)	Mn (%)	P (%)	S (%)	Ni (%)	Cr (%)
Rail	0.8	0.28	1	0.04 ma x.	0.05 max	-	-

Table 3.2: Mechanical properties of the rail material.

Material	Yield Stress (MPa)	Ultimate Tensile Strength (MPa)	Young's Modulus (GPa)	Poison's Ratio	Density (kg/m3)
Rail	540	780	207	0.3	7800

3.2. Specimen Dimension and Fatigue Testing Unit for Experimental Analysis

3.2.1. Specimen position on the Rail and Specimen Dimension

The specimen dimension and sampling position is prepared by the standard of National Standards of the People's Republic of China, GB 2585-2007with testing method of GB/T 3075 [36]. The specimen samples are taken from the head and foot of the rail with the positions shown below in figure 3.2.

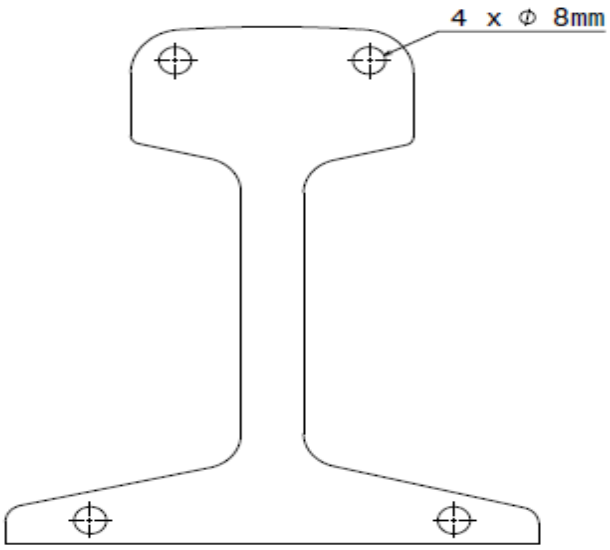

Figure 3.1: Position of the specimens in the rail

Fatigue failures occur at notches or stress concentrations. Almost all mechanical components and structural members contain some form of geometrical or micro-structural discontinuities. These discontinuities, or stress concentration factors, often result in maximum local stresses, σ_{max} that are many times greater than the nominal

stress, σ of the member. Figure 3.3 shows a sketch of a specimen and its dimensions (mm) used for both ANSYS and experimental analysis.

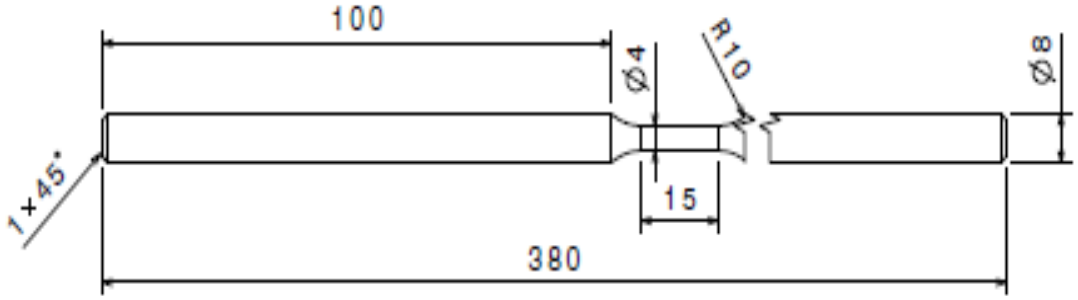

Figure 3.2: Un-notched Specimen Dimension

3.2.2. Fatigue Testing Unit Machine

Fatigue is a type of failure which results from cyclic loading at stress levels below the ultimate strength (i.e. the point at which a statically loaded sample would fracture). Fatigue damage is the cumulative effect of many small plastic deformations that occur during cyclic loading [34]. It is generally thought of as having three stages. Crack initiation is when micro-cracks form in areas with stress raisers or defects, like notches or rough surface features. Crack growth is when these cracks propagate and finally fracture is appeared when a dominant crack leads to sudden material failure. Fatigue Life (N_f) is defined as the number of stress cycles or strain reversals that a material experiences prior to fracture, and is simply the sum of the periods for the 3 stages mentioned, but since fracture is nearly instantaneous, it is usually omitted.

$$N_f = N_i + N_g, \text{ [cycles]} \quad 3.1$$

Where N_i corresponds to crack initiation and N_g corresponds to crack growth.

For this experiment, the stress-control fatigue test is performed and the fatigue property of rail specimens under different stress amplitudes is examined.

The apparatus used for the experiment is fatigue test unit machine. It is possible to determine the basic principles of the fatigue strength testing. On the lower panel of the unit, it is fixed an electric motor which axis is joined to an end of the test specimen (test bar) by means of a coupling. As well, this axis has a coupled disc, which by means a device will count the number of turns of the motor.

On the panel's right side, it is placed the system with which the test specimen is loaded. This system is composed by a spring balance, which is joined to a threaded spindle by its upper end, while on its lower side, it is joined to an articulated guided system, in which it is held the right side of the test specimen. When turning the threaded spindle clockwise, we transmit a vertical force upwards to the test specimen. The applied force can be directly measured using the spring balance.

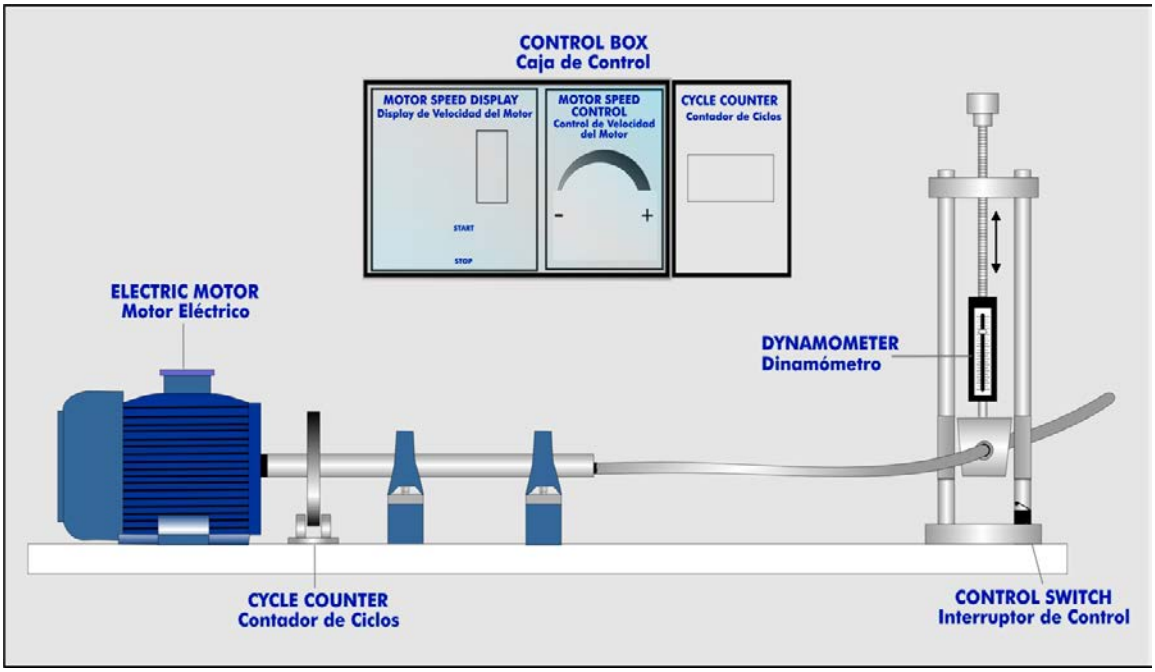

Figure 3.3: Fatigue testing unit process diagram and element allocation

In order to guarantee the force verticality, the system has two guides to avoid horizontal displacements during the transmission of stress. Likewise, in order to assure the constant application of the load, besides of allowing the test specimen rotation on its axial axis, the system also permits the alignment of the coupling with the test specimen, due to the deformity suffered by bending.

Both the area where the test specimen is located and the motor axis outcome are covered with a protection cover, without it the unit does not work, since it is provided with a safety system to avoid accidents. On the upper panel, the unit control box is mounted, containing: the main (on/off) switch of the unit; the cycle counter that shows us the

quantity of turns the motor's axis carries out; the motor's speed control that permits us increase or diminish the turning speed of the electric motor; the motor speed display that shows us the frequency in Hz, which is being transmitted to the motor at every moment; and the on/off switch of the electric motor (Refer the Appendix).

The objective of a fatigue test is generally speaking to determine the fatigue life and/or the damage points, i.e. the location of failure of a test-piece subjected to a prescribed sequence of stress amplitude. To determine the fatigue strength of materials, there are several kinds of fatigue tests, in different ways, for instance: single or rotating bending fatigue tests, tension or compression tests, torsion or even multi-axial fatigue tests (combined loadings). Fatigue tests show the time or number of cycles that a component will resist under cyclic loading, or the maximum bearable stress without failure before a given number of cycles. The method that is used for this experiment is constant amplitude test. This is the simplest sequence of amplitude obtained by applying reversals of stress of constant-amplitude to the test-piece until failure occurs. Different specimens of the test series may be subjected to different stress amplitude but for each individual item, the amplitude will never be varied.

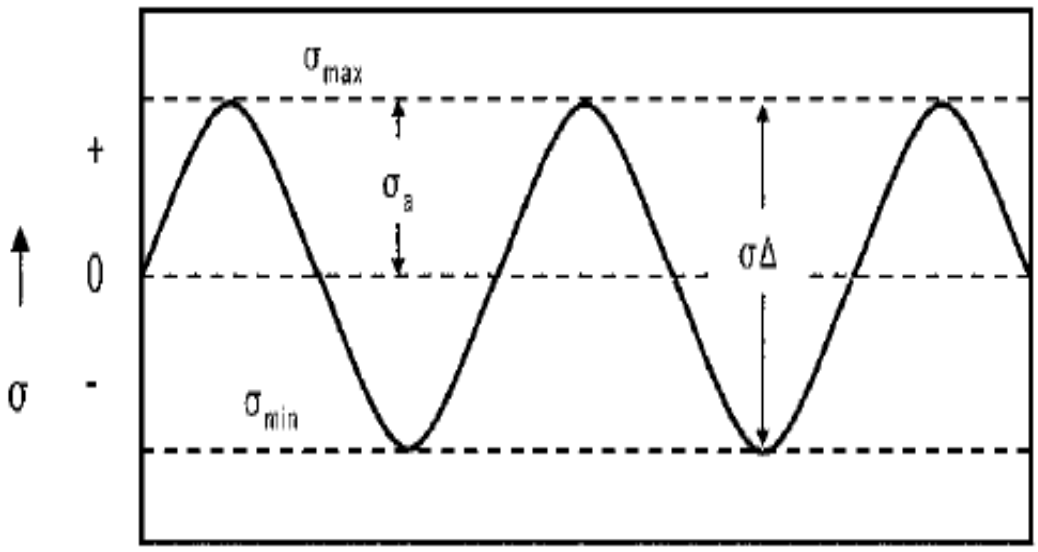

Figure 3.4: Fully reversed cyclic loading.

In fatigue testing, the applied stress, σ_a, is typically described by the stress amplitude of the loading cycle and it is defined as,

$$\sigma_a = \frac{\sigma_{max} - \sigma_{min}}{2} \quad 3.2$$

The stress amplitude is generally plotted against the number of cycle to failure to a linear-log scale, S-N plots. An S-N curve (Stress vs. Number of cycles) can be presented in terms of stress amplitude or maximum stress vs. the number of cycles (Figure 3.5). Such kind of curve is sometimes also called the Wohler curve, in attribution to the work of August Wohler in Germany in the 1850s.

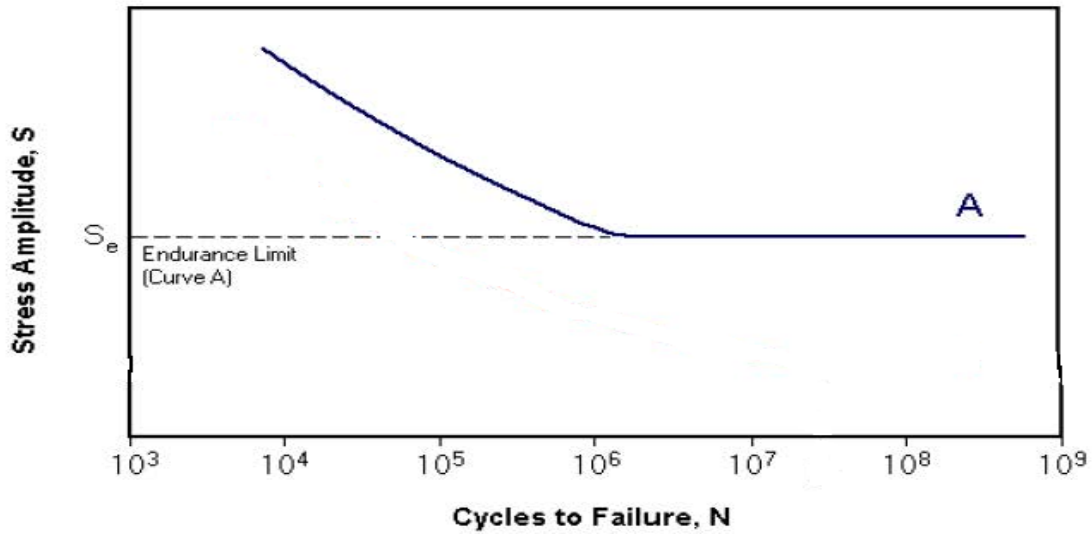

Figure 3.5: Stress vs. Number of cycles curve

3.3. Main Operation and Technical Conditions

3.2.1. Natural Environment in Addis Ababa Region

Altitude: ≤2500m

Ambient temperature: 0℃～+29.7℃

Average daily highest temperature in years: 25.5℃

Average daily lowest temperature in years: 6.1℃

Average relative humidity in year 95%

Average annual rain fall: 1000-1600mm

Maximum daily rain fall: 47mm

3.2.2. Main Parameters of Lines

Track gauge: 1435mm

Minimum radius of horizontal curve:

Mainlines between sections 50m

Yard line 30m

Minimum radius of vertical curve: 1000m

Maximum gradient: 55%

Type of rails for main lines and depot: 50kg/m

Empty vehicle load: 44 tones

Axle load: ≤11（1+3%）tones

3.2.3. Main Technical Indicators

Maximum operation speed: 70 km/h

Average travelling speed: ≥20 km/h

3.2.4. Main Dimensions of Wheel and Rail

The principal rolling radii of the wheel: $R_1^w = 330$ mm

The principal transverse radii of the wheel: $R_2^w = \infty$

The principal rolling radii of the rail: $R_1^r = \infty$

The principal transverse radii of the rail: $R_2^r = 300$ mm

(Source: Ethiopian Railway Corporation, Technical Specifications of Vehicles July 2013.)

3.4. Wheel/Rail and Rail Specimen Analysis Methods

From elementary mechanics, it is known that two contact surfaces under load will deform. Depending on the magnitude of the load applied and the materials' hardness, the deformation may be either plastic or elastic. For many engineering applications, the contact surfaces are non-conformal. The resulting contact areas are very small and the resulting pressures very high. The stresses on those contact surfaces can be determined from analytical formulas.

3.4.1. Hertzian Contact Theory

Wheel/rail contact phenomena results in stick slip wear, giving rise to crack initiation and its propagation to yield catastrophe. The contact condition in terms of contact pressure found to be more important than the grade of steel. Assessment of contact stresses at the wheel/rail interface thus poses a very important issue in a study of wheel/rail contact phenomena. It is important to understand here that wheel/rail contact pair's profile radii change with time and wear. This has drawn much attention of many researchers to investigate the problem mainly by means of theoretical or numerical approaches for the solution of Hertz theory [35]. Hertz contact theory appeared in 1881 to solve the problem of pressure distribution between two elastic spherical bodies in contact. Later he extended it to general case of two elastic bodies in contact. Then onwards researchers have used this theory for the analysis of the wheel/rail contact problem numerically to reach a more realistic solution. The contact-pair topology influences the contact stress magnitude and shape of contact area. Hertz theory has its own limitations in the assumptions. Hertz's model of contact stress relies on the following simplifying assumptions:

- The materials in contact are homogeneous.
- Contact stress is caused by the load which is normal to the contact tangent plane, which implies that there are no tangential forces acting between the solids.
- The contact area is very small compared with the dimensions of the contacting solids.
- The contacting solids are at rest and in equilibrium.
- The effect of surface roughness is negligible.

The configuration of two elastic bodies with convex surfaces in contact is the basis of Hertz's theory.

3.4.2. Analysis of Load Distribution and 3D Contact

If two elastic nonconforming bodies contact together then according to the Hertz contact theory, the contact area is elliptical in shape with a major semi-axis a and a minor semi-axis b [32].

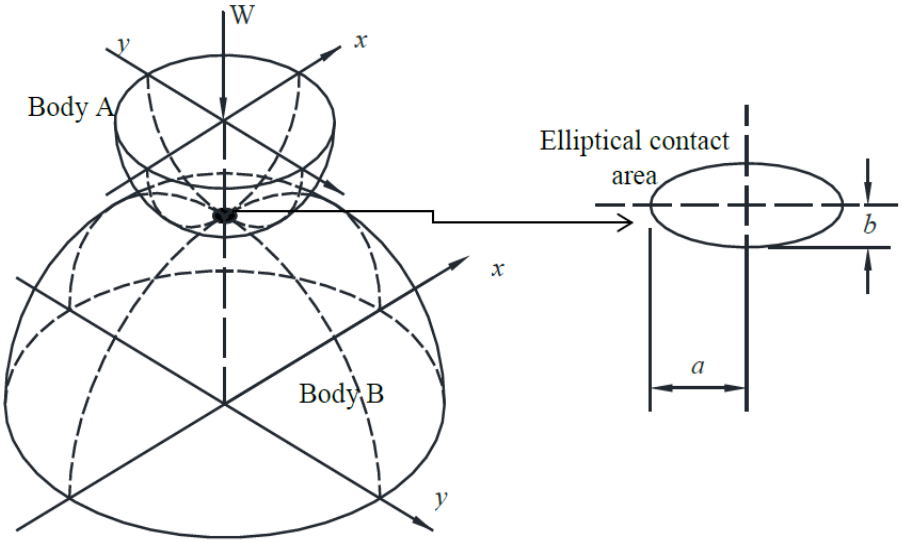

Figure 3.6: Geometry of two elastic bodies with convex surfaces in contact.

When considering two elastic bodies in contact, as shown in Figure 3.7, they will meet at a single point *O*, where the normal distance between them is zero. Near this contact point, without load, the body surface shapes may be represented by two second-order polynomials:

$$Z_1 = A_1x^2 + B_1y^2 \quad 3.3$$

$$Z_2 = A_2x^2 + B_2y^2 \quad 3.4$$

The coefficients A_1, A_2 and B_1, $B_2$are assumed to be constant.

The general conditions considered during the wheel rail contact simulation are the assumption of the Hertz contact theory. As explained in the previous chapter the common Hertz assumptions are:

- ✓ Isotropic and homogenous material
- ✓ No friction (The surfaces of both bodies had to be completely smooth)
- ✓ Both bodies were considered as half-spaces
- ✓ The contact is elastic.

In the case of a railway, the four main curvatures can be considered to be in perpendicular planes. Their directions correspond to the main axes of the frame: *O-xy*.

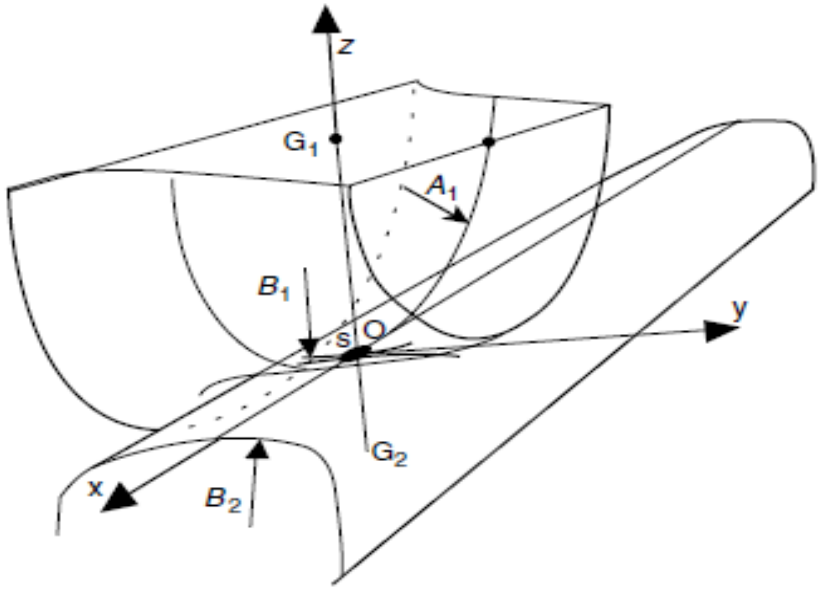

Figure 3.7: Hertzian contact: the railway case.

In the 3D railway case, the above-mentioned curvatures and radii will be:

Wheel: $\frac{d^2Z_1}{dx^2} = 2A_1 = \frac{1}{R_{1w}}$ 3.5

Wheel: $\frac{d^2Z_1}{dy^2} = 2B_1 = \frac{1}{R_{2w}}$ 3.6

Rail: $\frac{d^2Z_2}{dy^2} = 2B_2 = \frac{1}{R_{2r}}$ 3.7

Where R_{1^w} is the longitudinal radius of the wheel at the contact point, R_{2^w} is the transversal radius of the wheel profile and R_{2^r} is the transversal radius of the rail profile. In the railway case, the curvature A_2 is generally neglected as the rail principal rolling radius R_{1^r} is ∞.

Before being loaded, the vertical relative distance $d(x,y)$ between the two bodies can be written as:

$$Z_1 + Z_2 = d(x,y) = Ax^2 + By^2 \quad 3.8$$

With

$$A = \frac{1}{2r_n}, \text{ and } B = \frac{1}{2}\left(\frac{1}{R_{wx}} + \frac{1}{R_{rx}}\right) \quad 3.9$$

A and B are principal curvature of the two bodies and strictly positive.

According to Hertzian contact theory, the contact area of a wheel and rail is elliptical in shape, with the major and minor semi-axis a and b respectively (Figure 3.7). The contact pressure distribution P in this area can be expressed as:

$$P = \frac{3F_n}{2\pi ab}\sqrt{1 - \left(\frac{x}{a}\right)^2 - \left(\frac{y}{b}\right)^2} \quad 3.10$$

Where, F_n is the applied normal load at the contact, a and b are semi axes of the contact ellipse, the magnitudes of a and b depend on the normal load, wheel and rail profiles and materials. X and Y are the required coordinates to specify the point of contacts on the rail surface based on the lateral rail surface parameter.

The contact ellipse semi-axes a and b are determined as follows:

$$a = m\left(3\pi F_n(K_w + K_r)|4K_3\right)^{\frac{1}{3}} \quad 3.11$$

$$b = n\left(3\pi F_n(K_w + K_r)|4K_3\right)^{\frac{1}{3}} \quad 3.12$$

According to these assumptions and by using equation (3.10) the maximum contact pressure, P_0 (Hertz stress) occur at x=0 and y=0.

$$P = P_0 = \frac{3F_n}{2\pi ab} \quad 3.13$$

Depending on the size and orientation of the contact ellipse the positions of the contact point may be shifted in different directions based on the magnitude of x or y. However, based on the above general Hertz contact formula and assumptions, the stress due to wheel/rail contact decreases and becomes zero if it goes far away from the centerline of the rail head. Similarly, the wheel/rail contact stress is inversely proportional to the major and minor axis of the contact ellipse.

To calculate a and b, first let's find the values of K_w, K_r and K_3.
K_w and K_r are constants that depend on the material properties of railway wheel and rail respectively.

Where

$$K_w = \frac{1-(v^w)^2}{\pi E^w} \tag{3.14}$$

and

$$K_r = \frac{1-(v^r)^2}{\pi E^r} \tag{3.15}$$

Where v^w and E^w are Poisson's ratio and young's modulus of the railway wheel material and v^r, and E^r are Poisson's ratio and young's modulus of railway rail material.

$$K_w = \frac{1-(0.3)^2}{\pi \times 207 \times 10^9 N/m^2}, \quad K_w = 1.4 \times 10^{-12}\frac{m^2}{N}$$

Also

$$K_r = \frac{1-(v^r)^2}{\pi E^r}$$

$$K_r = \frac{1-(0.3)^2}{\pi \times 207 \times 10^9 N/m^2}, \quad K_r = 1.4 \times 10^{-12}\frac{m^2}{N}$$

$K_3$is a constant and depends on the geometric properties of the two bodies and is defined as follows,

$$K_3 = A + B = \frac{1}{2}\left(\frac{1}{{R_1}^w} + \frac{1}{{R_2}^w} + \frac{1}{{R_1}^r} + \frac{1}{{R_2}^r}\right) \tag{3.16}$$

R_1^{w} and R_1^{r}, are the principal rolling radii of the wheel and the rail respectively and R_2^{w} and R_2^{r}, are the principal transverse radii of curvature of the wheel and rail respectively.

$$K_3 = \frac{1}{2}\left(\frac{1}{330\,mm} + \frac{1}{\infty} + \frac{1}{\infty} + \frac{1}{300\,mm}\right), \qquad K_3 = 0.0032/mm$$

The coefficients m and n are Hertz coefficients and they are given as a function of the angle θ (0^0– 90^0) where θ is defined as:

$$\theta = \cos^{-1}\left(\frac{K_4}{K_3}\right) \tag{3.17}$$

And

$$K_4 = B - A = \frac{1}{2}\sqrt{\left(\frac{1}{{R_1}^w} - \frac{1}{{R_2}^w}\right)^2 + \left(\frac{1}{{R_1}^r} - \frac{1}{{R_2}^r}\right)^2 + 2\left(\frac{1}{{R_1}^w} - \frac{1}{{R_2}^w}\right)\left(\frac{1}{{R_1}^r} - \frac{1}{{R_2}^r}\right)\cos 2\varphi} \tag{3.18}$$

φ is the angle of the orientation difference of the principle axes of the two bodies; also called yaw rotation. For a straight segment the curvature of the rail, $\varphi = 0^o$. Therefore,

$$K_4 = \frac{1}{2}\sqrt{\left(\frac{1}{330} - \frac{1}{\infty}\right)^2 + \left(\frac{1}{\infty} - \frac{1}{300}\right)^2 + 2\left(\frac{1}{330} - \frac{1}{\infty}\right)\left(\frac{1}{\infty} - \frac{1}{300}\right)\cos 2(0^o)}$$

$$K_4 = 0.1515 \times 10^{-3}/mm$$

For a straight rail segment, θ is defined as:

$$\theta = \cos^{-1}\left(\frac{K_4}{K_3}\right)$$

$$\theta = \cos^{-1}\left(\frac{0.1515 \times 10^{-3}}{0.0032}\right), \qquad \theta = 87.3^0$$

By using the Hertz coefficient table and linear interpolation method the value of m and n for the selected rail can be easily obtained.

Table 3.3: Hertz coefficients.

θ (deg)	**m**	**n**	θ (deg)	**m**	**n**	θ (deg)	**m**	**n**
0.5	61.4	0.1018	10	6.6	0.311	60	1.49	0.72
1	36.89	0.1314	20	3.81	0.413	65	1.38	0.76
1.5	27.48	0.1522	30	2.73	0.493	70	1.28	0.8
2	22.26	0.1691	35	2.4	0.53	75	1.2	0.85
3	16.5	0.1964	40	2.14	0.567	80	1.13	0.89
4	13.31	0.2188	45	1.93	0.604	85	1.06	0.94
6	9.79	0.2552	50	1.75	0.641	90	1	1
8	7.86	0.285	55	1.61	0.678			

(Source: Investigation of surface ratcheting due to rail/wheel contact (2013).)

By interpolation method, we can calculate m and n

$\theta_1 = 85^0$,m_1=1.06, n_1= 0.94, $\theta_2 = 90^0$ m_2= 1.0, n_2= 1.0

$$m = m_1 + \frac{m_2 - m_1}{\theta_2 - \theta_1}(\theta - \theta_1)$$

$$m = 1.06 + \frac{1 - 1.06}{90 - 85}(87.3 - 85\ )$$

$$m = 1.0324$$

Similarly,

$$n = n_1 + \frac{n_2 - n_1}{\theta_2 - \theta_1}(\theta - \theta_1)$$

$$n = 0.94 + \frac{1 - 0.94}{90 - 85}(87.3 - 85\ )$$

$$n = 0.9676$$

Now, the values of a and b are:

$$a = m\left(3\pi F_n(K_w + K_r)|4K_3\right)^{\frac{1}{3}}$$

But, the axle load is ≤ 11(1+3%） tones.

Axle Load = (11+0.33) tones = 11330 kg.

The normal load (force) applied on each wheel is half of the axle load multiplied by the gravitational acceleration, that is:

$$F_n = \frac{Axle\ Load\ * g}{2} = \frac{11330 \times 10}{2} = 56650\ N$$

Then,

$$a = 1.0324\left(3 \times \pi \times 56650 \frac{\left(2 \times 1.4 \times 10^{-12}\ \frac{m^2}{N}\right)}{4 \times \frac{0.0032}{m}}\right)^{\frac{1}{3}}$$

$$a = 0.0083m$$

$$b = n\left(3\pi F_n (K_w + K_r)|4K_3\right)^{\frac{1}{3}}$$

$$b = 0.9676\left(3 \times \pi \times 56650 \frac{\left(2 \times 1.4 \times 10^{-12}\ \frac{m^2}{N}\right)}{4 \times \frac{0.0032}{m}}\right)^{\frac{1}{3}}$$

$$b = 0.0047m$$

By using the values of a, b and the normal force, the maximum Hertz contact stress will be:

$$P = P_0 = \frac{3F_n}{2\pi ab}$$

$$P_0 = \frac{3 \times 56650}{2 \times \pi \times 0.0083 \times 0.0047}$$

$$P_0 = \ 693.4MPa$$

The maximum contact pressure of 693.4 MPa is less than the ultimate tensile strength of rail, so the rail can resist the pressure applied at the contact area. The angular velocity of the wheel with maximum operating speed of the vehicle is:

$$\omega = \frac{v}{R_{1w}}$$

Where v is the maximum operation speed of the vehicle, 70km/hr = 19.44m/s and R_{1^w} is the principal rolling radius of the wheel, 300mm = 0.33m.

$$\omega = \frac{19.44}{0.33} = 58.92\ rad/s$$

3.4.3. Wheel/Rail Analysis with ANSYS 12.0

In order to build a realistic model of wheel/rail contact problem a 3D elasto-plastic finite element model is needed. This model should be able to accurately calculate the 3D stress response in the contact region as well as includes both material and geometric nonlinearity. The model is constructed by CATIA V5 software and imported to ANSYS 12.0 workbench.

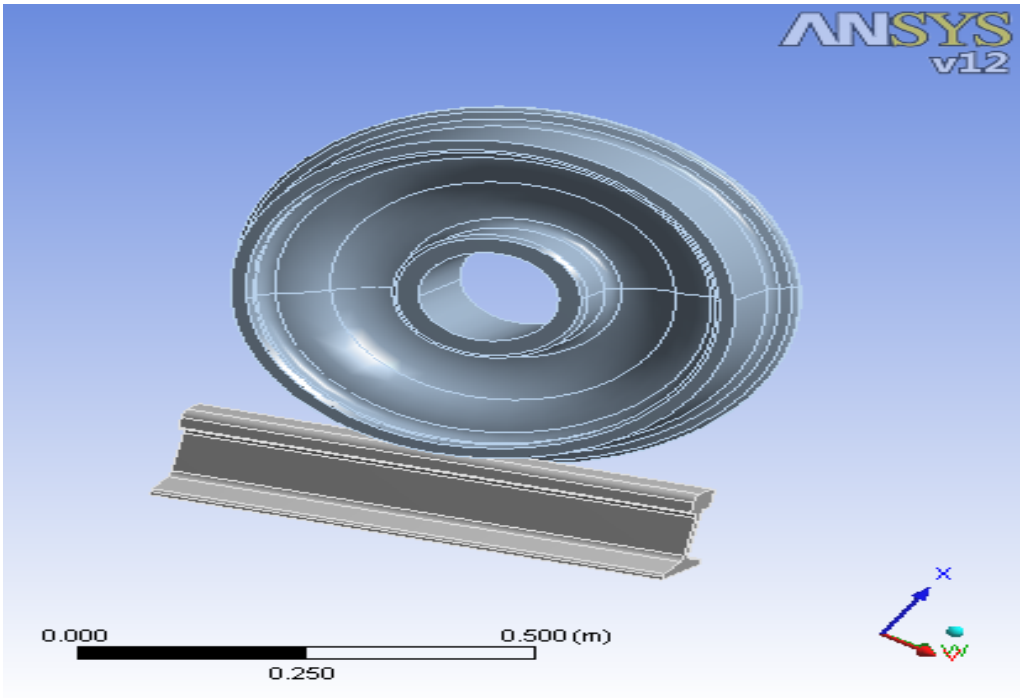

Figure 3.8: Wheel/rail contact model with CATIA V5

For this fatigue life analysis test, we are going to use one side wheel and rail model. After giving the connection bond between wheel and rail, meshing of both parts follow.

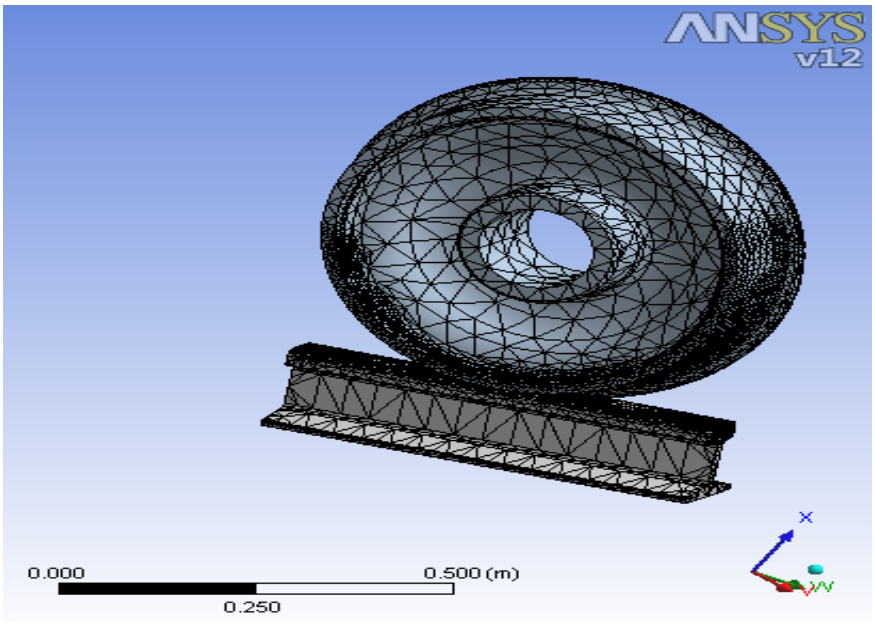

Figure 3.9: Wheel/rail meshing

Fixed boundary condition is applied to the rail at the bottom of the foot. Force is applied on the wheel and the rotational velocity of the wheel is applied to the wheel center. Also the standard earth gravity is applied.

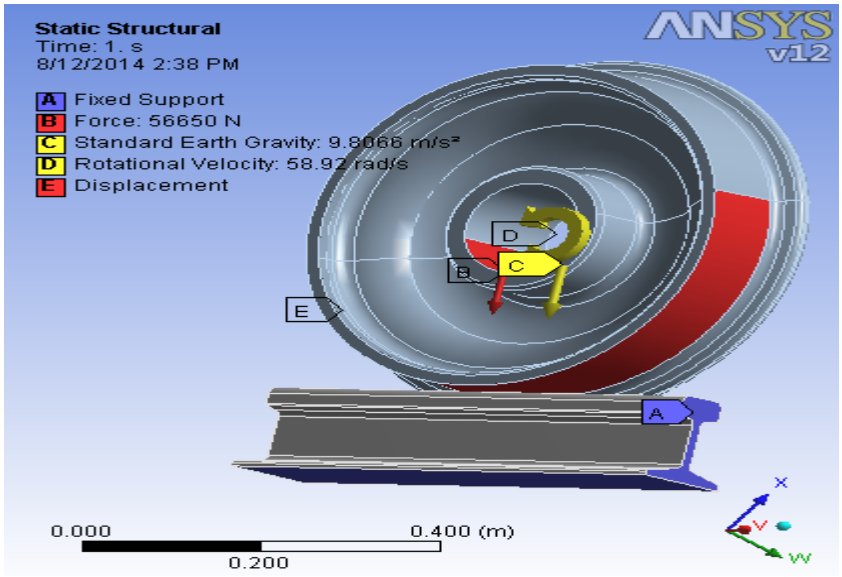

Figure 3.10: Wheel/Rail boundary conditions and input data

3.4.4. Numerical and Experimental Analysis of Specimen Fatigue Life

The specimen modeling is done by CATIA V5 and imported to ANSYS 12.0 for analysis purpose (Figure 3.11 (a)). The dimension (length 380mm, maximum and minimum diameter 8 and 4 mm respectively) is similar with the specimen used in the experiment. The meshing method is tetrahydrons with 1133 nodes and 466 elements (Figure 3.11 (b)).

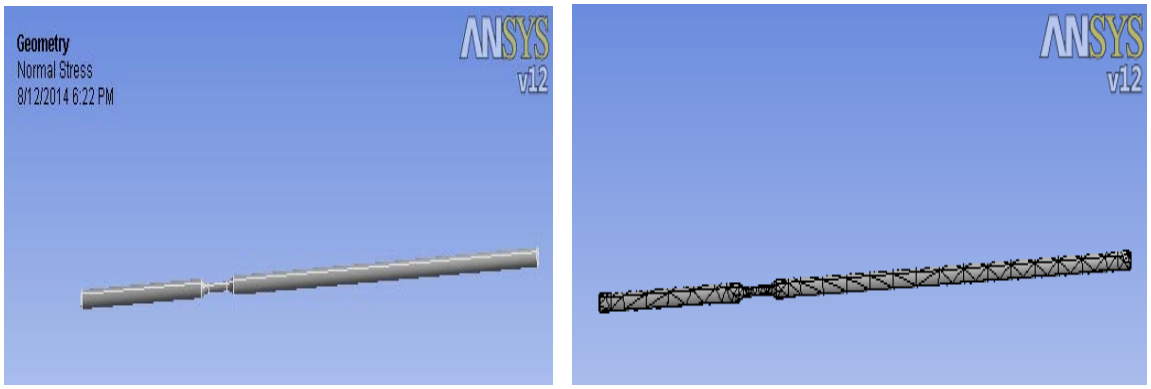

(a) (b)

Figure 3.11: Specimen modeling and mesh

The input data for the each specimen is shown below in the figures. In figure 3.12 (a), specimen 1 with rotational velocity, 45 N applied force, standard earth gravity, displacement and fixed support is shown similarly figure 3.12 (b) shows the specimen 2 with 40 N, rotational velocity, standard earth gravity, displacement and fixed support at one side of the specimen.

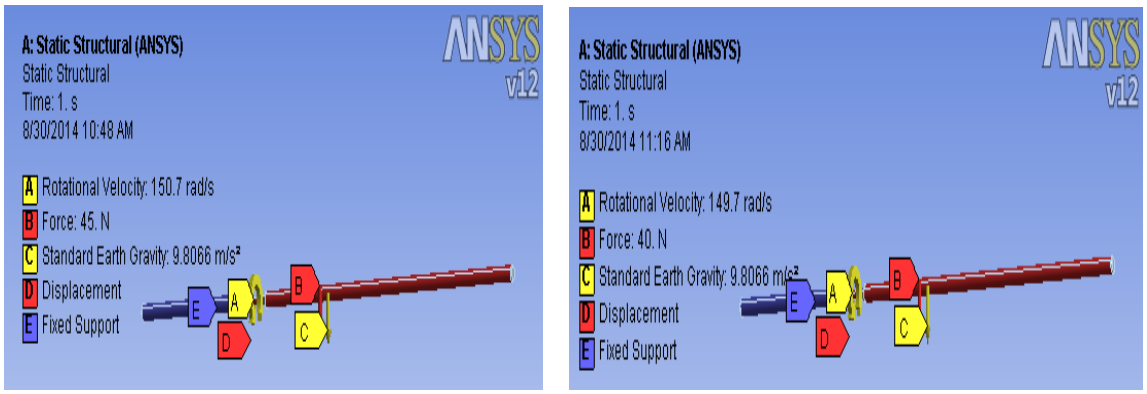

(a) (b)

Figure 3.12: Specimen 1 (a) and 2 (b) boundary conditions and input data

Similarly, specimen 3 input data with the applied load of 35 N is shown in figure 3.13 (a) and specimen 4 input data and boundary conditions with the applied load of 26.7 N is demonstrate In figure 3.13 (b).

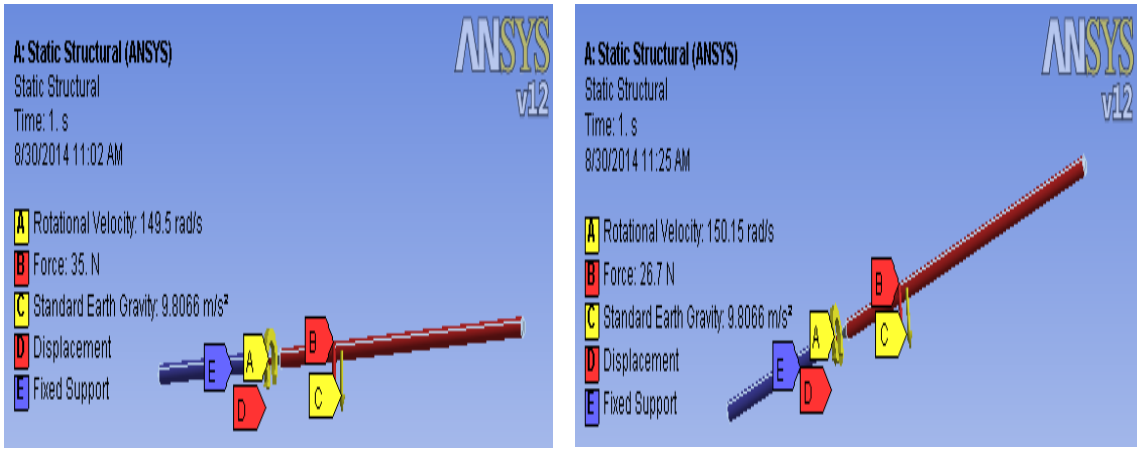

(a) (b)

Figure 3.13: Specimen 3 (a) and 4 (b) boundary conditions and input data

For the experimental part, four specimens are cut out from the rail and machined by leath machine and prepared. The dimension of each specimen is with length of 380mm, maximum diameter of 8mm and minimum diameter of 4mm. The experimental analysis is done by applying different load step by step on fatigue testing unit machine after one specimen is failed.

Figure 3.14: Specimen for experimental analysis

Figure 3.15 shows the testing machine with the specimen. The specimen is placed in the floating bearing and collet chuck then tightens the screw and mounts the protective hood and lock. The force applied is the same value (4.5 kg, 40kg, 35kg and 2.67kg) with the analysis on ANSYS 12.0.

Figure 3.15: Specimen placed in the fatigue testing unit machine

CHAPTER FOUR: RESULT AND DISCUSSION

4.1. Result

Wheel/Rail Result

For wheel/rail fatigue life analysis, there are some outputs from the ANSYS software. The results found are mentioned below.

Equivalent Elastic Strain:

In the figures 4.1 below, the maximum and minimum values of equivalent elastic strain is on the rail (1.3067 x 10^{-3} maximum and 0.0001647 x 10^{-3} minimum values).

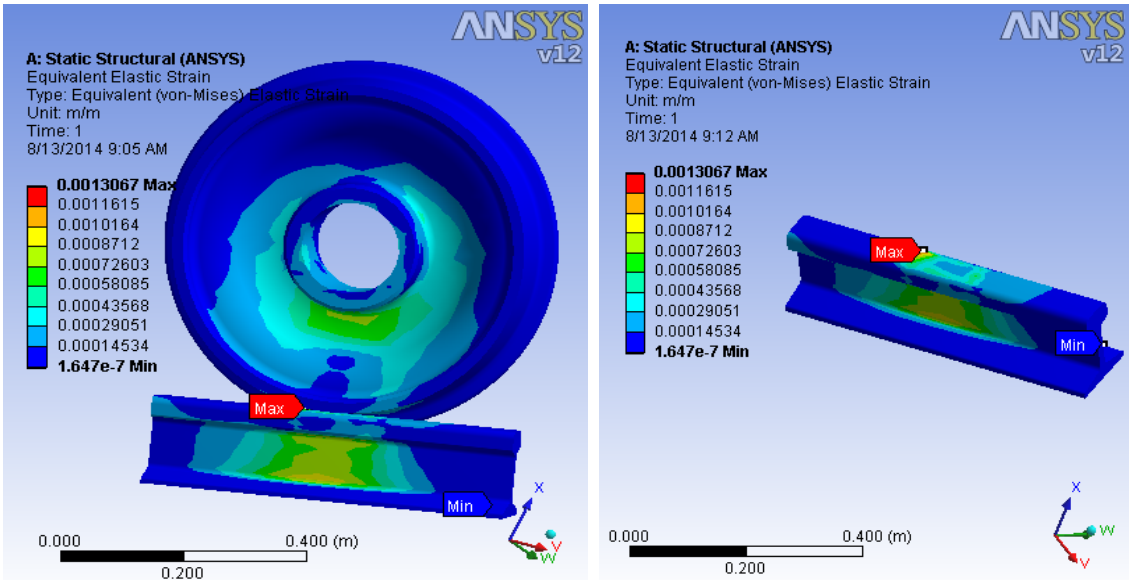

Figure 4.1: Contour plot of equivalent elastic stress

General Fatigue Results

Fatigue Life

Fatigue Life can be over the whole model or scoped just like any other contour result in Workbench (i.e. parts, surfaces, edges, and vertices). Figure 4.2 shows the available life for the given fatigue analysis. The minimum fatigue life is on the rail and its value is 1000000 cycles and the maximum value is 57748 cycles.

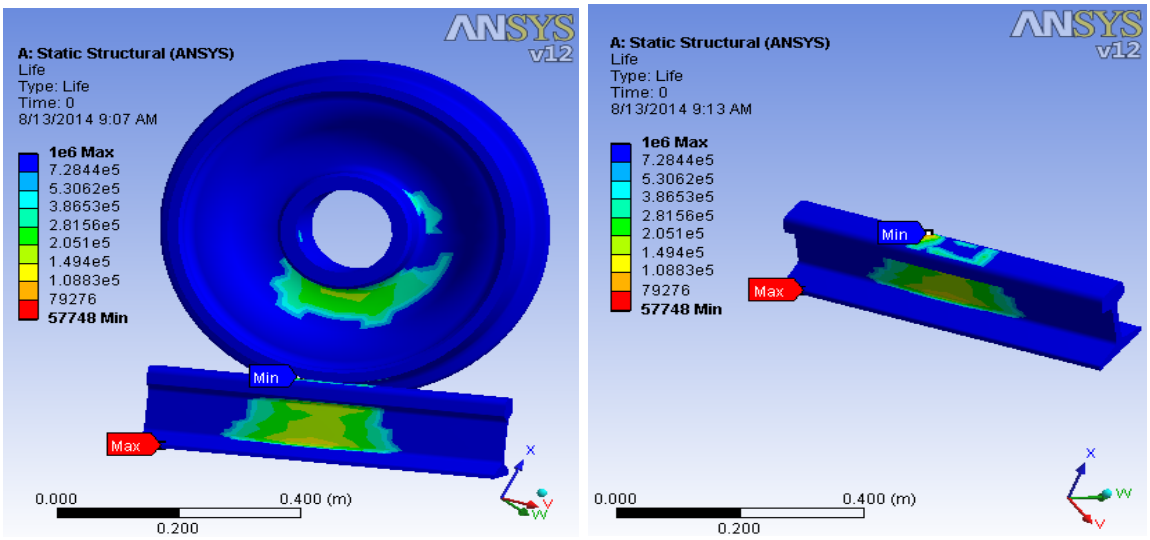

Figure 4.2: Contour plot of fatigue life over the whole model

Equivalent Alternating Stress

In a Stress Life fatigue analysis, one always needs to query an SN curve to relate the fatigue life to the stress state. Thus the “equivalent alternating stress” is the stress used to query the fatigue

SN curve after accounting for fatigue loading type, mean stress effects, multi-axial effects, and any other factors in the fatigue analysis. The maximum equivalent alternating stress shown in figure 4.3 is 261.34 MPa.

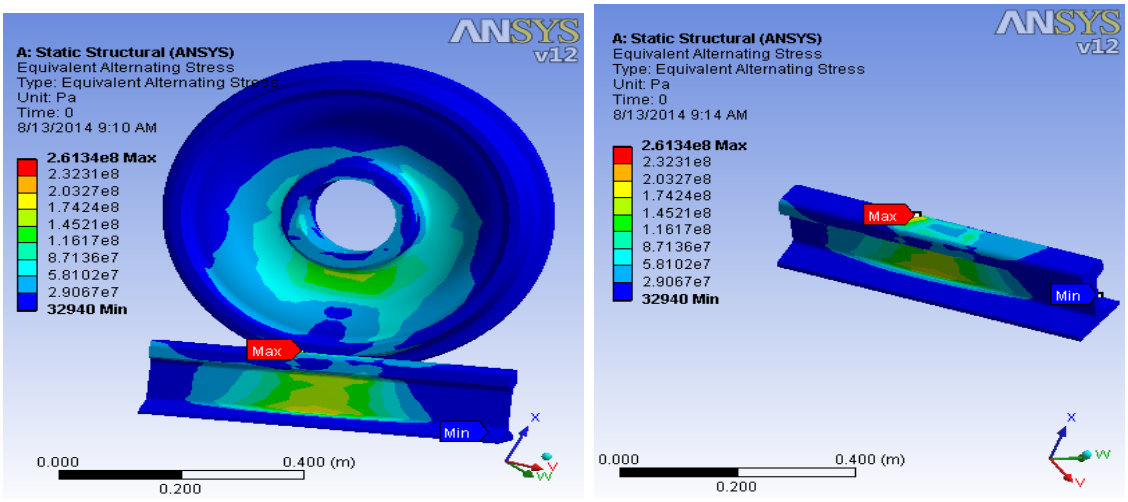

Figure 4.3: Contour Plot of Equivalent Alternating Stress

Fatigue Sensitivity

Figure 4.4 shows fatigue sensitivity curve and how the fatigue results change as a function of the loading at the critical location on the model. This result may be scoped. Sensitivity may be found for life, damage, or factor of safety.

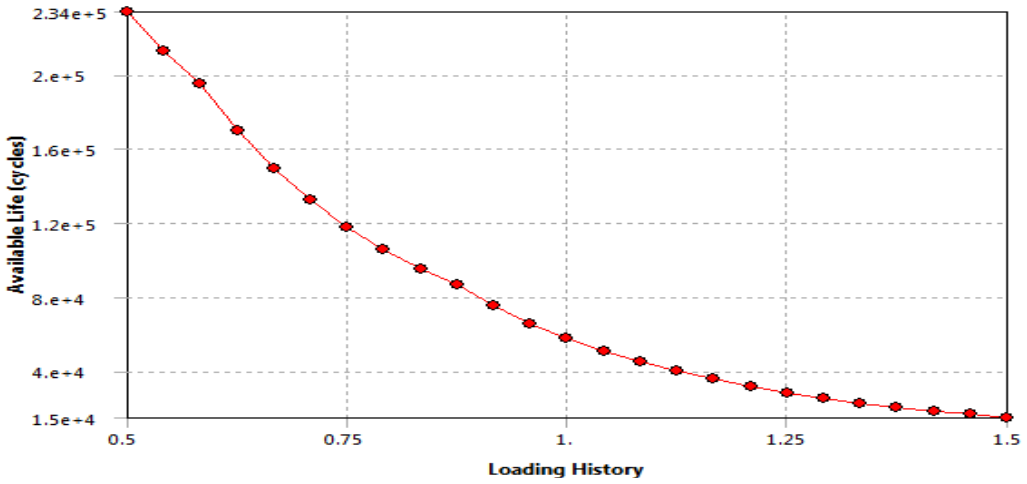

Figure 4.4: Fatigue Sensitivity Curve.

Specimen ANSYS Result

- **Structural analysis results for specimen 1 at 45N**

Fatigue Life

Out of the four specimens, Specimen 1 is loaded with 45N. The maximum fatigue life of this specimen is 1000000 cycles and the minimum is 1055.2 cycles is demonstrated in figure 4.5.

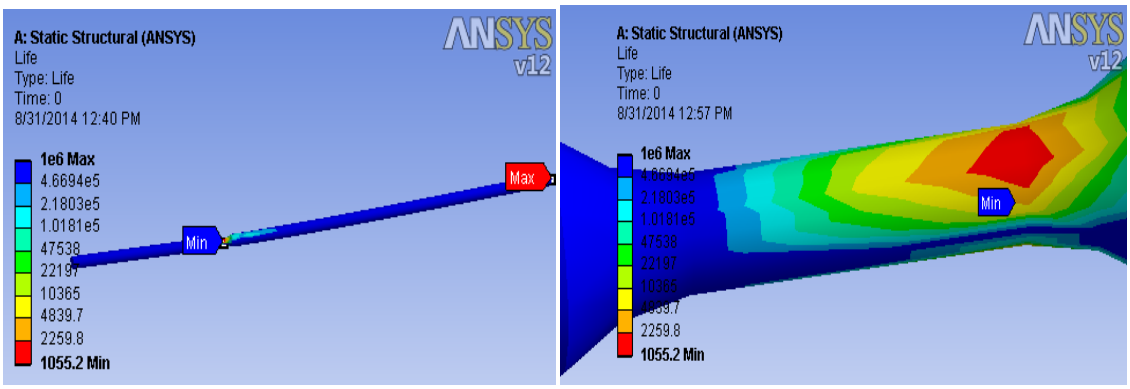

Figure 4.5: Fatigue life of the specimen 1 at 45N

Equivalent Alternating Stress

The maximum value of equivalent alternating stress for specimen 1 is 480.35x10^6 MPa and the minimum value is 5244.9 Pa shown in figure 4.6.

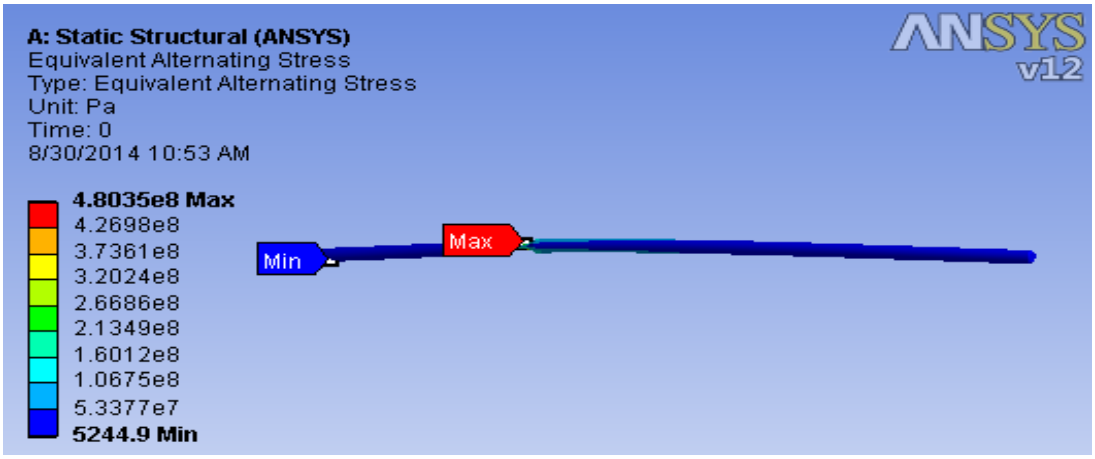

Figure 4.6: Equivalent alternating stress of the specimen 1 at 45

- **Structural analysis results for specimen 2 at 40N**

Fatigue Life

Figure 4.7 and 4.8 shows the fatigue life (1000000 cycle maximum and 1601.4 cycle minimum) and the equivalent alternating stress (428.12 MPa maximum and 4687.2 Pa minimum). The minimum fatigue life and the maximum alternating stress is at the neck of the specimen.

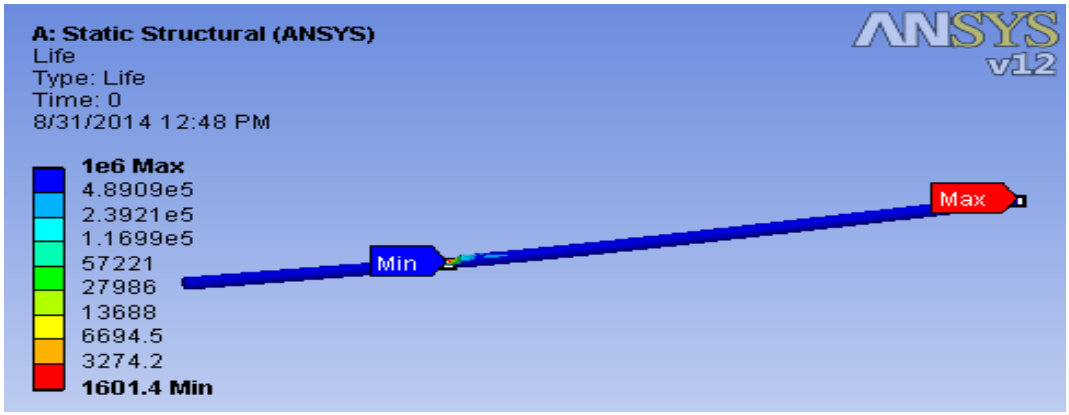

Figure 4.7: Fatigue life of the specimen 2 at 40N

Equivalent Alternating Stress

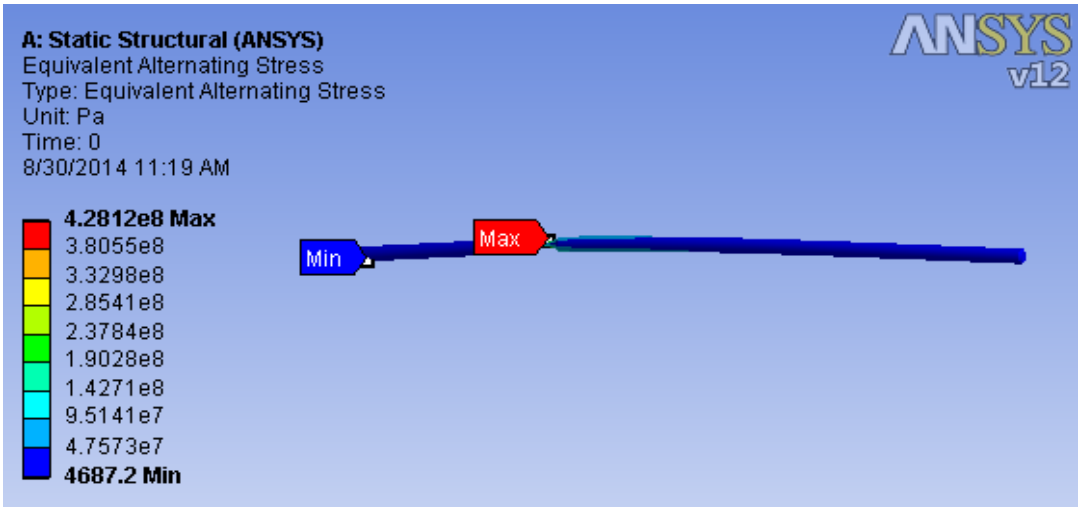

Figure 4.8: Equivalent alternating stress of the specimen 2 at 40N

- **Structural analysis results for specimen 3 at 35N**

Fatigue Life

Similarly, figures 4.9 and 4.10 below demonstrates the fatigue life of the specimen 3 (1000000 cycle maximum and 3277.2 cycle minimum values) and the equivalent alternating stress (375.88 MPa maximum and 4131.5 Pa minimum values). The minimum life and maximum alternating stress is at the neck of the specimen.

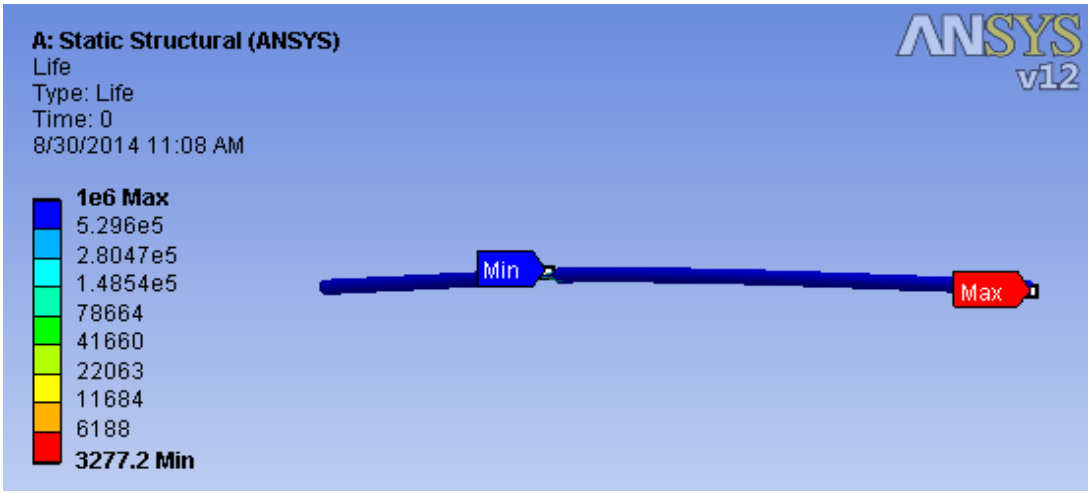

Figure 4.9: Fatigue life of the specimen 3 at 35N

Equivalent Alternating Stress

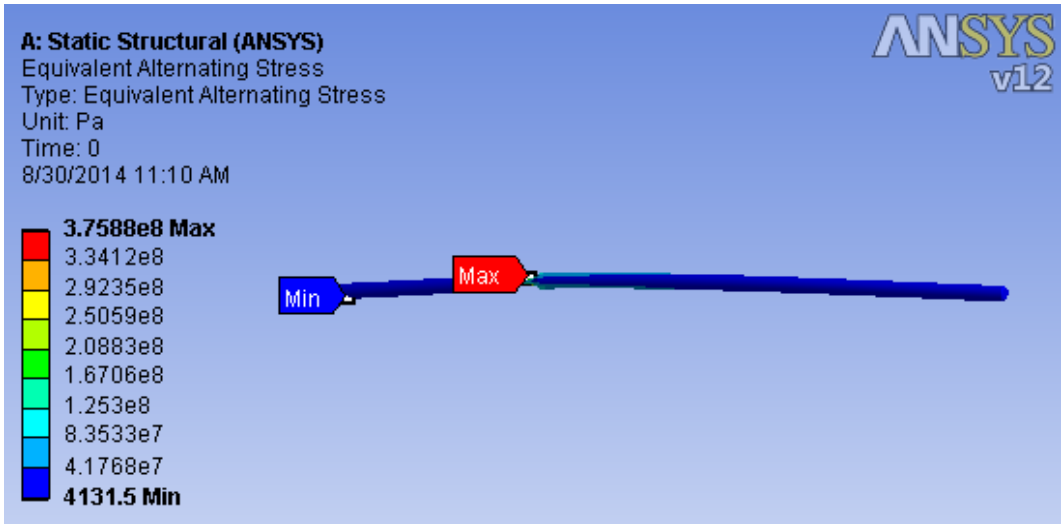

Figure 4.10: Equivalent alternating stress of the specimen 3 at 35N

- **Structural analysis results for specimen 4 at 26.7N**

Fatigue Life

Finally, the specimen loaded with 26.7 N fatigue life is shown in Figure 4.11. The maximum fatigue life for the specimen 4 is 1000000 cycle and the minimum value is 7371.1 cycle.

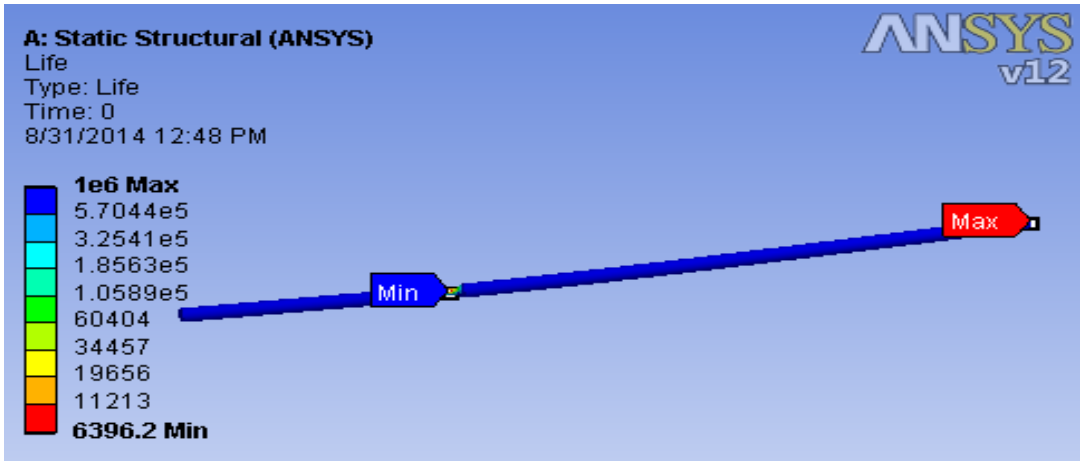

Figure 4.11: Fatigue life of the specimen 4 at 26.7N

Equivalent Alternating Stress

The equivalent alternating stress maximum value of 289.17 MPa maximum and 3213.3 minimum value is shown in figures 4.12.

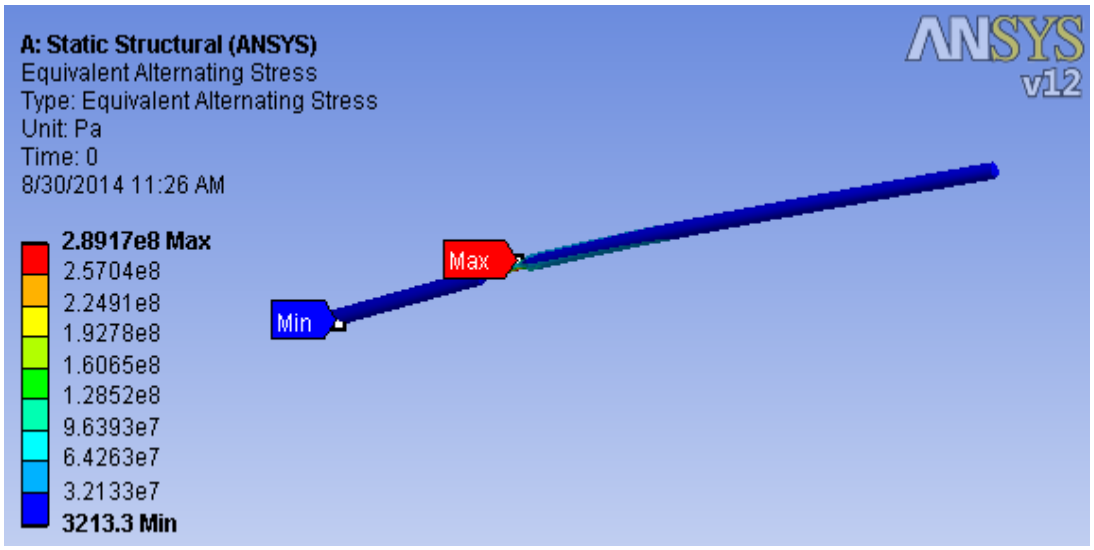

Figure 4.12: Equivalent alternating stress of the specimen 4 at 26.7N

Specimen Experimental Result

The first specimen is inserted in the machine and applies the load, unfortunately the specimen is failed suddenly. The reason is that at the time of machining, the specimen surface finish was not smooth at the filleted region so that the stress concentration on this area makes it to fail fast. At the machining process, we are trying to correct this surface but it will reduce the stepped diameter so can't do it.

The second specimen is loaded to 4.0 kg. After rotating to 1864 cycles, the specimen is failed. Figure 4.13 show the load applied (SF-1), cycle count (count) and the motor speed (SV-1).

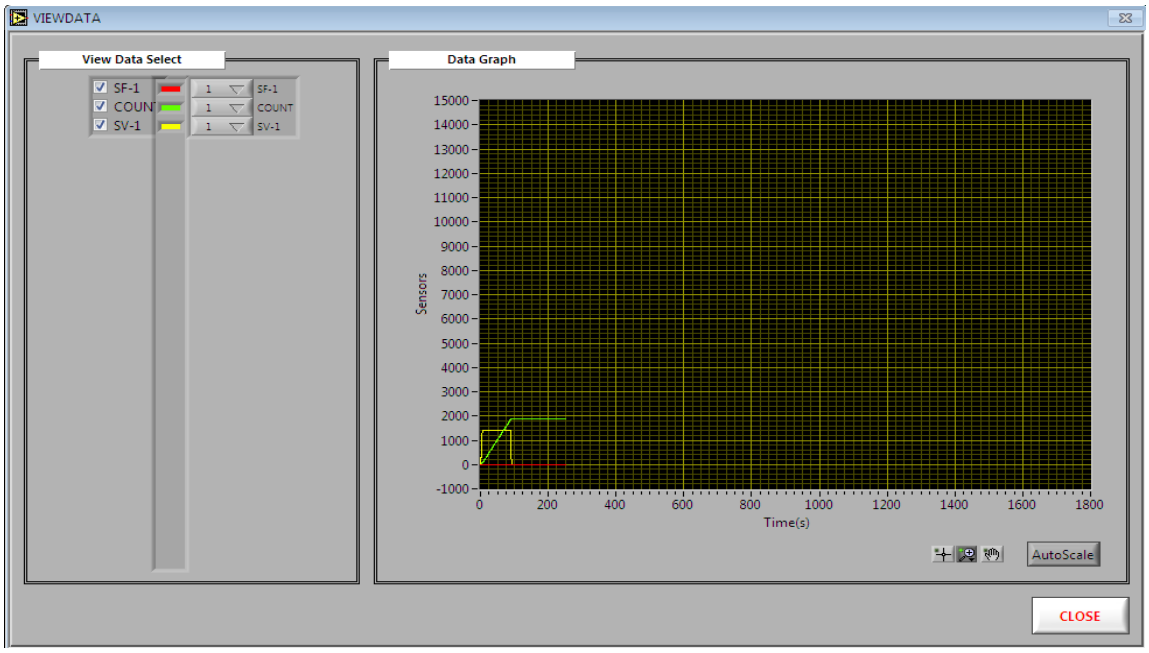

Figure 4.13: Experimental output of specimen 2

The third specimen is placed in the machine and adjusts the load to 3.5 kg to start the experiment. After rotating to 4660 cycles, the specimen is failed. The load applied (SF-1), cycle count (count) and the motor speed (SV-1) is shown in figure 4.14.

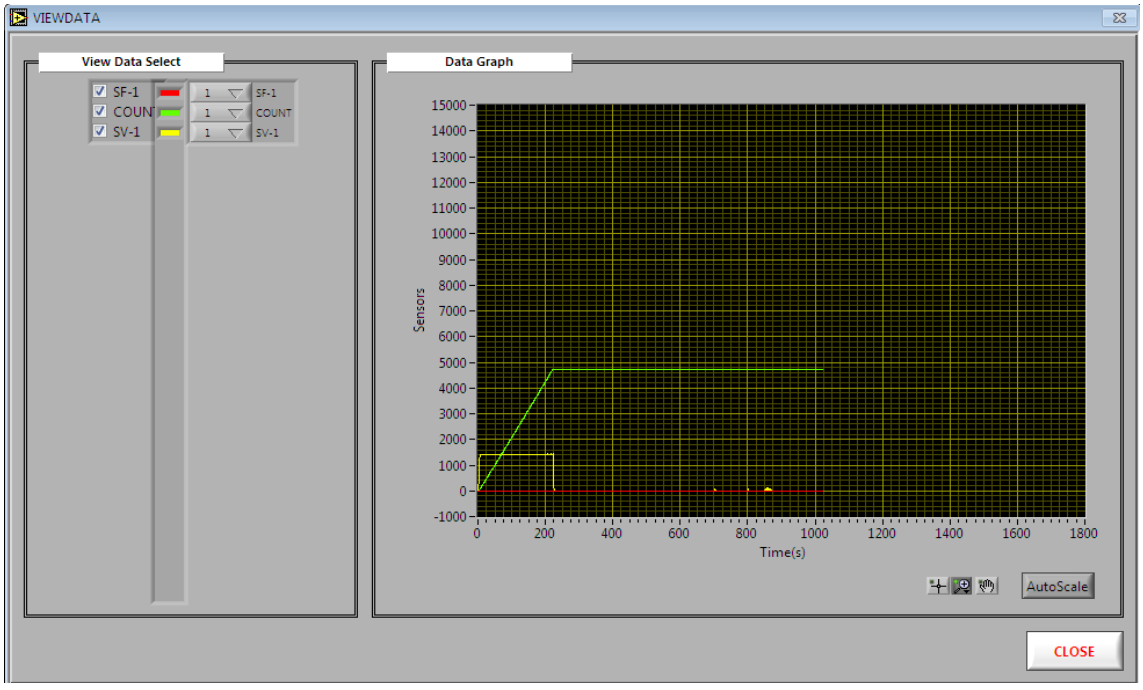

Figure 4.14: Experimental output of specimen 3

Finally, the last specimen is inserted to the machine and loaded with 2.67 kg and start the experiment, after a cycle of 6940 it failed. The load, count and speed of the motor is shown in figure 4.15.

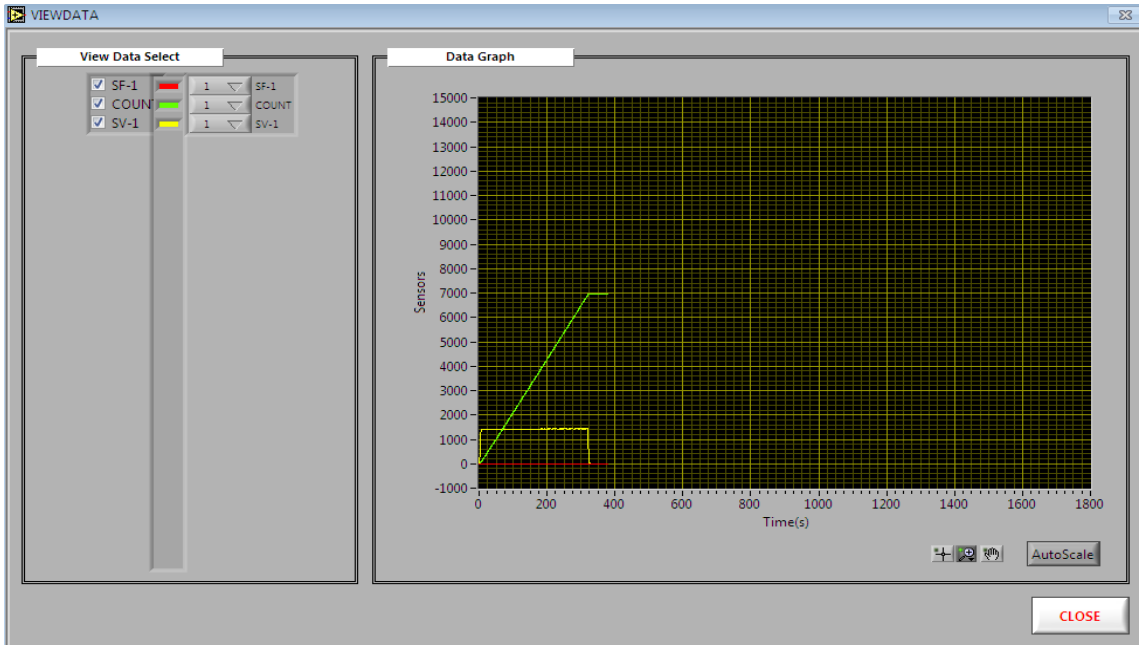

Figure 4.15: Experimental output of specimen 4

After conducting the experiment, the failed specimens found are shown bellow in figure 4.16.

Figure 4.16: Specimens failed on fatigue test

4.2. Discussion

This paper focuses on the wheel/rail fatigue life and the fatigue life comparison between the specimens modeled in ANSYS and experimental result. Or the rolling contact fatigue failure analysis at wheel/rail contact model in ANSYS predicts that the maximum value of the equivalent alternating stress decreases, in contrast to that of the fatigue life (Figure 4.17).

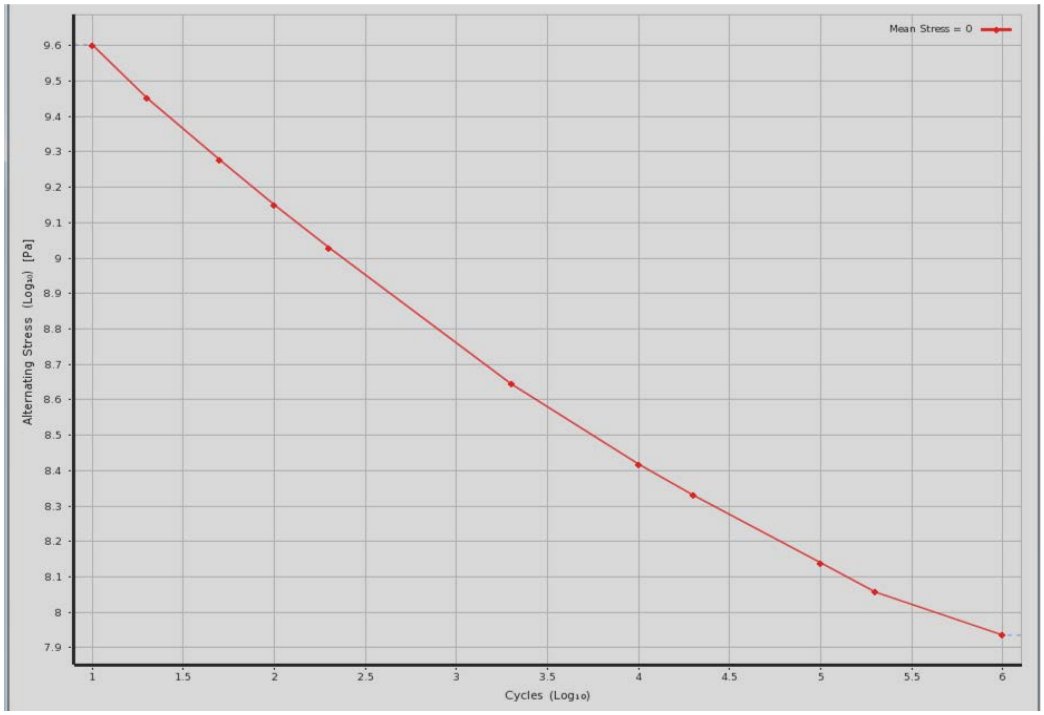

Figure 4.17: Stress vs Fatigue life curve for wheel/rail ANSYS result

The result found on the specimen by ANSYS and experimental methods is summarized in table 4.1.

Table 4.1: Summary of data obtained from ANSYS and Experimental

Load (N)	Specimen minimum diameter, D (mm)	Alternating Stress, S (MPa)		Fatigue Life, N (Cycle)	
		ANSYS	Experimental	ANSYS	Experimental
26.7	4	289.17	318.5	6396.2	6940
35	4	378.88	417.5	3277.2	4730
40	4	428.12	477.2	1601.1	1864
45	4	480.35	-	1055.2	-

For both cases, the equivalent alternating stress is increases as the load increases. In contrary as the load increases, the fatigue life is decreasing, it means the more load is applied the fatigue life of the rail will be smaller and smaller. It is seen from the table that, the better analysis of fatigue life is by experimental method with attention to the preparation of the specimen.

The comparison of load applied and fatigue life is shown in figure 4.18 for ANSYS and experimental results.

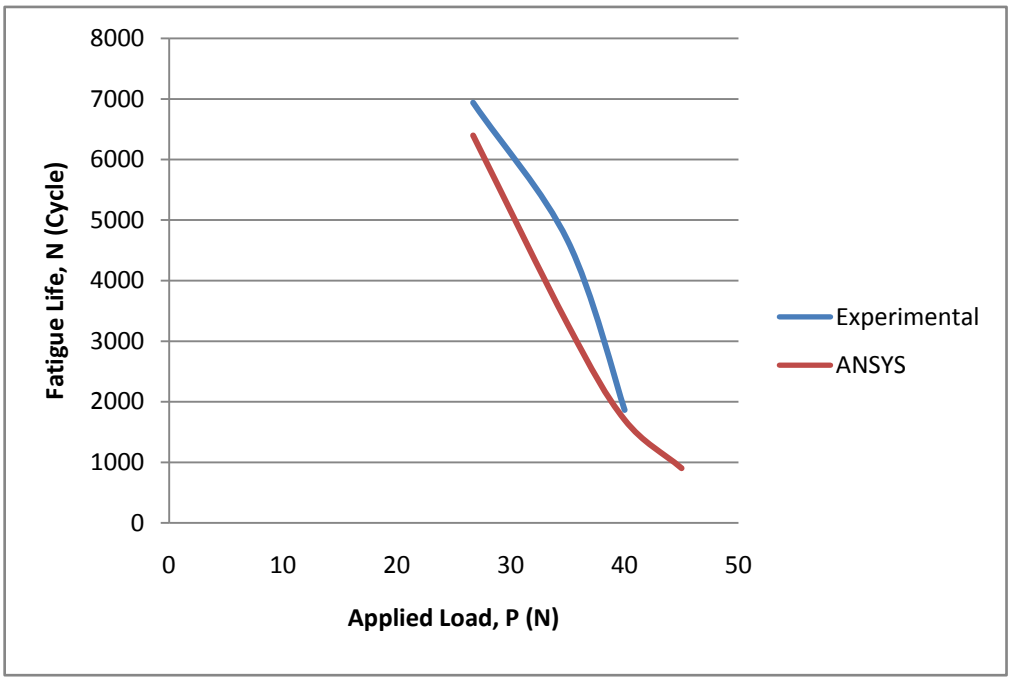

Figure 4.18: Comparison of applied load vs Fatigue Life Curve

The graph shows the experimental analysis is better than the ANSYS result. But the experimental analysis curve is not uniform at the middle. This is because of the specimen surface finish of the specimens.

CHAPTER FIVE: CONCLUSION, RECOMMENDATION AND FUTURE WORK

5.1. Conclusion

The purpose of this paper is analysis of rolling contact fatigue and show the fatigue life of wheel/rail due to the cyclic axle load applied. Also the fatigue life comparison of the rail between ANSYS software and experimental test on the samples prepare from the rail. Four specimens are preparing for the experimental test. By applying different loads (2.67, 35, 40 and 45 kg), the cycle to failure is determined on the fatigue testing unit machine. With the same loading condition and specimen model, the fatigue life analysis is done by ANSYS software. From both approach, as the load applied increases the life of the rail decreases. By the output of the analysis, the result found by the experimental is enhanced than that of ANSYS. Even if the experimental result is better, there are some gaps on the conducted experiment. The specimens must have a good surface finish but it can't be found all in all. This is perhaps due to the lack of skill of the persons who prepared the specimen and the precision of the lathe machines used. In conclusion as far as fatigue life of rail is concerned, the suitable cyclic axle load and proper maintenance before crack initiate and propagate may be regarded as the best possible life improvement operation.

5.2. Recommendation

From the result found from experimental and ANSYS methods, the best way of analyzing fatigue life is in experimental analysis. The test has a better fatigue life for the same applied loads at each case. We can see that as the applied load increases the life of the rail decreases. In this manner there are some recommendations given for the Ethiopian railway corporation. Predicting and preventive maintenance will help to increase the crack initiation and crack propagation and minimize the cost of maintenance of rail change due to damage. Increasing the life of crack initiation and propagation means improving the total fatigue life of the rail itself. Additionally by using better strength material property than the AA light rail transit used, the fatigue life of the rail will be improved.

5.3. Future Work

During the analysis of rolling contact fatigue at rail, there are a lot of problems to be solved. However, because of the broad applications of fatigue failure mechanics, in this paper the analysis is limited to the fatigue life of rail by experimental and ANSYS software due to the effect of applied axle load. However identifying the place of failure, failure causes and considering different types of truck play a great role on the future works of minimizing rolling contact fatigue problems.

Finally, some suggestions are listed below for future work as extension and continuity of this paper.

- Analysis of rolling contact fatigue failure with different truck conditions. (Like curved, transition).
- For the FE analysis, by using the full licensed ANSYS software, crack initiation and crack propagation analysis of rolling contact fatigue can be done.
- Develop more fatigue strength material.
- Identify and improve the life of crack initiation and propagation.
- Management of rolling contact fatigue with different parameters.
- Influences of rolling contact fatigue on surface damage and wear.

Reference

[1] Akeel, N.A., M.A. Aziman, Zainuddin Sajuri, Ahmad Kamal Ariffin, A.W. Ikhsan, Identification of Damages and Stress Analysis of Rail/Wheel Rolling Contact Region. Key Engineering Materials, 2011, pp: 462-463.

[2] Marine Vidaud, Willem-Jan Zwanenburg, Current situation on rolling contact fatigue – a rail wear phenomenon, Conference paper STRC, 2009.

[3] Wikipedia, The Free Encyclopedia, History of Rail Transport, 2012, August 20 2014, http://en.wikipedia.org/wiki/History of rail transport.

[4] Wikipedia, The Free Encyclopedia, Rail Transport in Ethiopia, 2012, August 20 2014, http://en.wikipedia.org/wiki/Rail transport in Ethiopia.

[5] Eric Magel, Peter Sroba, Kevin Sawley and Joe Kalousek, Control of Rolling Contact Fatigue of Rails, Conference paper, 2004.

[6] Davis, C., L., "Modelling and Detecting Damage (Wear and RCF) in Rails", Prepared for Rail Safety and Standard Board, School of Engineering, University of Birmingham, 2003.

[7] Pradeep Kumar Garg, Rolling Contact Fatigue and its Management with Emphasis on Rail Grinding, Seminar 2011.

[8] Matthew Rudas, John Baynham, Robert A.Adey, Simulation of wheel-rail damage, 2013.

[9] Nagaraj K. Arakere,A Review of Rolling Contact Fatigue, Journal of Tribology, October 2009, Vol. 131.

[10] R A Smith,Rolling Contact Fatigue of Rails, Imperial College of Science, Technology and Medicine, London, 2001, 25-29.

[11] Kumaran,G., D. Menonand K.K. Nair, Dynamic Studies of Rail Track Sleepers in a Track Structure System. Journal of Sound and Vibration, 2003, 268: 485-501.

[12] Venkatarami Reddy, Development of an Integrated Model for assessment of operational risks in rail track, 2007.

[13] European Commission DGX111 Brite/Euram III Project, Integrated Study of Rolling Contact Fatigue (ICON), Contract BRPR-CT96-0245 Project Programme, Brussels, 1997-1999.

[14] The Versailles Railway Accident of 1842 and the Beginnings of the Metal Fatigue Problem, Smith, R.A . In Proceedings Fatigue 90, The Fourth International Conference on Fatigue and Fatigue Thresholds, Hawaii , July 15-20 1990, Eds. H. Kitagawa and T. Tanaka, Materials and Component Publications Ltd., Birmingham, Vol. 4, 1990, pp2033-2041.

[15] Olver, A., V., The Mechanism of Rolling Contact Fatigue: An Update, Proceedings of the Institution of Mechanical Engineers, Part J: Journal of Engineering Tribology,2005, Vol. 219, No. 5, pp. 313-330.

[16] Ekberg, A. &Kabo, E., Fatigue of Railway Wheels and Rails under Rolling Contact and Thermal Loading-An Overview, Wear, 2005, Vol.258, pp.1288-1300.

[17] Chue, C., H., Chung, H., H. , Lin, J., F. & Chou, C., C., 2001, “The Effect of Strain Hardened Layer on Pitting Formation During Rolling Contact”, Wear, Vol. 249, pp. 109-116.

[18] Ringsberg, J., W., “Life Prediction of Rolling Contact Fatigue Crack Initiation”, International Journal of Fatigue, 2001, Vol. 23, pp. 575-586.

[19] Fletcher, D., I., Franklin, F., J. &Kapoor, A., Image Analysis to Reveal Crack Development using a Computer Simulation of Wear and Rolling Contact Fatigue, Fatigue & Fracture of Engineering Materials and Structures, 2003,Vol. 26, pp. 957-967.

[20] Brennan, F., P. &Teh, L., S., Determination of Crack-tip Stress Intensity Factors in Complex Geometries by the Composition of Constituent Weight Function Solutions, Fatigue & Fracture of Engineering Materials & Structures, 2004, Vol. 27, No.1, pp. 1-7.

[21] N.A. Akeel, Z. Sajuri and A.K. Ariffin, Analysis of Rolling Contact Fatigue Damage Initiation At The Wheel-Rail Interface, Australian Journal of Basic and Applied Sciences, 5(12): 2011, 937-945.

[22] Li, Y., Kang, G., Wang, C., Dou, P. & Wang, J., Vertical Short-Crack Behaviour and its Application in Rolling Contact Fatigue, International Journal of Fatigue, 2006, Vol. 28, No. 7, pp. 804-811.

[23] Farris, T., N., Keer, L., M. & Steele, R., K., Life Prediction for Unstable Shell Growth in Rails, Journal of Engineering for Industry, 1990, Vol. 12, pp. 175-180.

[24] Kim, J., K. &Kiim, C., S., Fatigue Crack Growth Behavior of Rail Steel Under Mode I and Mixed Mode Loading, Material Science and Engineering, 2001, Vol. 338, pp. 191-201.

[25] Jeong, J., Y. &Orringer, O., Fatigue Crack Growth of Surface Cracks in the Rail Web, Theoretical and Applied Fracture Mechanics, 1989, Vol. 12, pp. 45-58.

[26]Olofsson, U. & Nilsson, R., Surface Cracks and Wear of Rail: a Full-Scale Test on a Commuter Train Track, Proceedings of Institute of Mechanical Engineers, 2002, Vol.216, Part F: Journal of Rail and Rapid Transit, pp. 249-264.

[27] Bhushan B., John Wiley & Sons, Principles and Applications of Tribology, New York, 1999.

[28] Lewis R. and Olofsson U. (Eds.), Wheel–Rail Interface Handbook, Woodhead Publishing Limited, Cambridge, UK, 2009.

[29] Kuna M., Springmann M., Mädler K., Hübner P., and Pusch G., Fracture mechanics of a railway wheel made of austempered ductile iron, Engineering Fracture Mechanics, 2005, 72, pp. 241–253.

[30] Jon Sundh, On wear transitions in the wheel-rail contact, Department of Machine Design, Royal Institute of Technology, Doctoral thesis, 2009.

[31] Jokipi K., Kymenite in railway applications. In: Conference Group of the ADI-Seminar, the 8th of November, Technical University in Helsinki, 1991, pp. 1–16.

[32] Munidasa Widhana, Investigation of Surface Ratchetting due to Rail/Wheel Contact, Doctoral thesis, 2013.

[33] Ringsberg J.W., Franklin F., Josefsson B.L., Kapoor A., and Nielsen J. C.O., Fatigue evaluation of surface coated railway rails using shakedown theory, finite element calculations and lab and field trials, International Journal of Fatigue, 2005, 27, pp. 680–694.

[34] K. Komvopoulos, Mechanical Testing of Engineering Materials, 2nd edn (San Diego, CA: University Readers), 2011.

[35] Jay Prakash Srivastava, P.K. Sarkar, Vinayak Ranjan, An Approximate Analysis for Hertzian Elliptical Wheel-Rail Contact Problem, Proceedings of the 1st International and 16thNational Conference on Machines and Mechanisms, 2013, 249-253.

[36]National Standards of the People's Republic of China, Hot-rolled steel rails for railway, GB 2585—2007.

Appendix

Fatigue Testing Apparatus

Function and layout

In the revolving fatigue testing machine, a rotating sample which is clamped on one side is loaded with a concentrated force. As a result, an alternating bending stress is created in the cylindrical sample.

Following a certain number of load cycles, the sample will rupture as a result of material fatigue.

The revolving fatigue testing machine essentially consists of

- Spindle with sample receptacle (1)
- Drive motor (2)
- Load device (3)
- Switch box with the electrical control and counter (4)
- Protective hood (8)

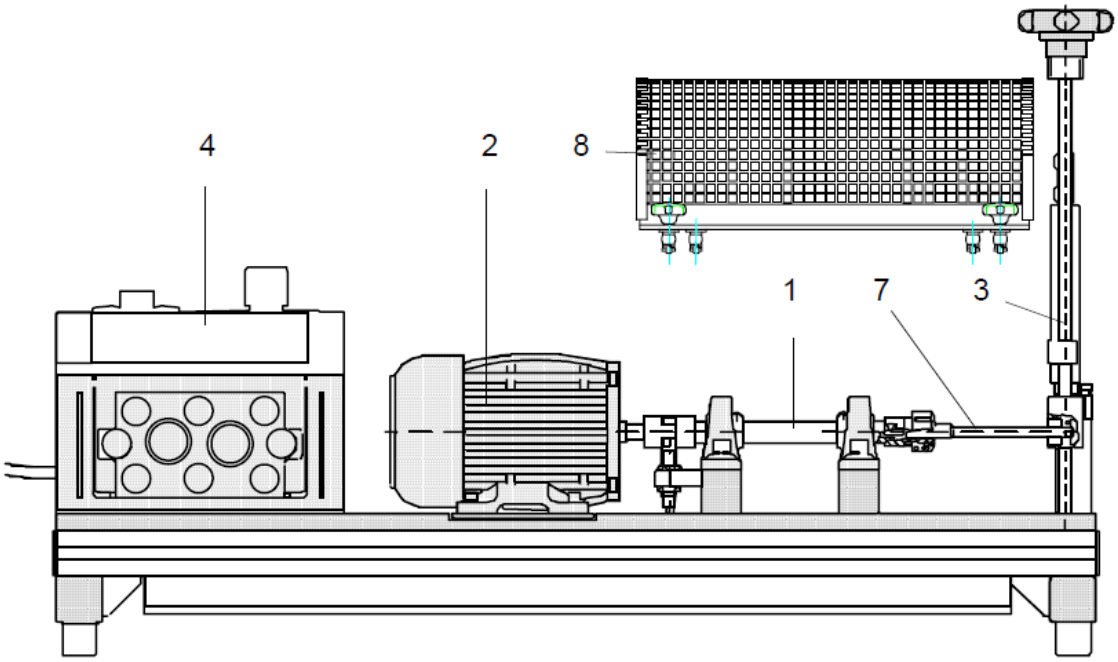

The specimen is mounted on two amply dimensioned rolling-contact bearings. The spindle is driven by a smooth running a.c. motor of 0.37 kW with maximum speed of 1500 rpm.

The procedures of each experiment run are determined as the following:

The test bar (7) is clamped in the spindle on one side by a collet chuck (5) and guided on the other side in a floating bearing (6)

Loading of the sample is performed using a spring balance (9) and the floating bearing (6).

Pre-stressing of the spring balance and hence adjustment of the load is performed via a threaded spindle with a hand wheel (10).

The set load can be read from the computer connected to the fatigue testing unit.

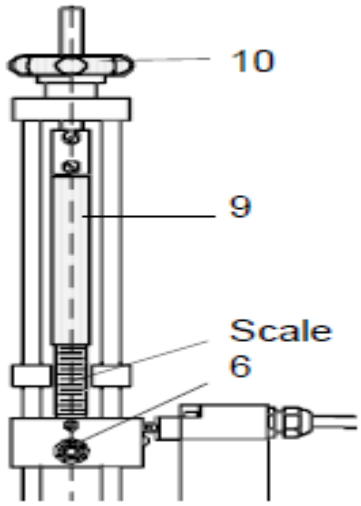

The pulses for the counter are supplied by an inductive proximity sensor (12) on the motor coupling.

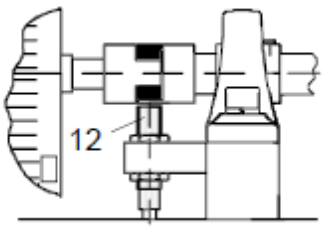

If the sample ruptures, the motor and the counter are halted automatically via the stop switch (16).

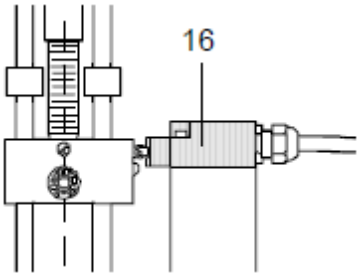

The master switch (13), emergency off switch (14), motor control switch (15) and counter (11) are housed in the switch box (4).

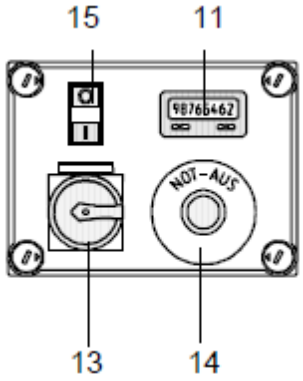

Experiments

Commissioning and test run

The following checks should be performed before carrying out experiments

- Erect the revolving fatigue testing machine and connect to the power supply
- Remove the protective hood (unlock the fasteners by rotating the knobs to the left)

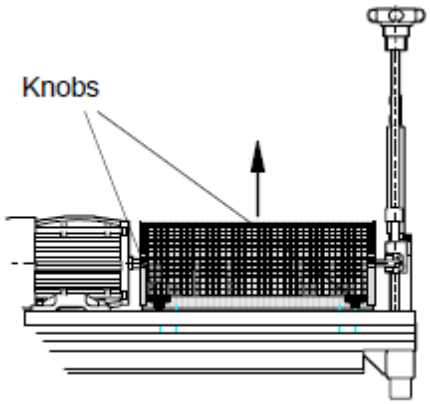

- Relieve the load device using the hand wheel (move the floating bearing down to the bottom)
- Remove any samples which may be in position
- Lightly tighten the union nut on the collet chuck

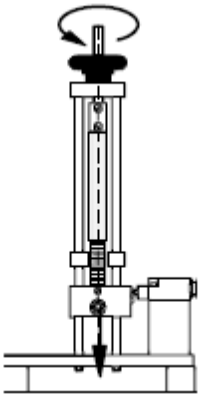

- Mount the protective hood and lock with all four knobs

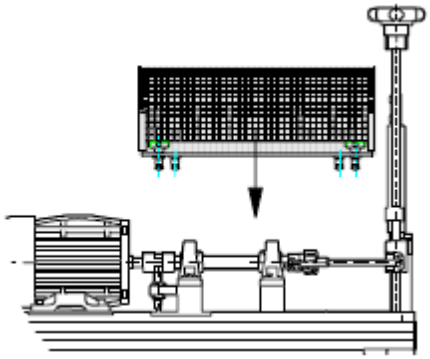

DANGER!

- Never operate the revolving fatigue testing machine without the protective guard! Parts of the sample could fly off when it ruptures. Rotating machine parts must be protected against accidental contact.

- Check whether the EMERGENCY OFF switch (14) is released (pull out)
- Switch on the machine using the master switch (13)

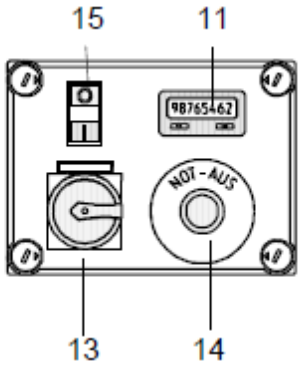

- Check whether the automatic stop device is functioning.

  To do so, raise the floating bearing on the load device by rotating the hand wheel. The motor should then be stopped by the stop switch (16)

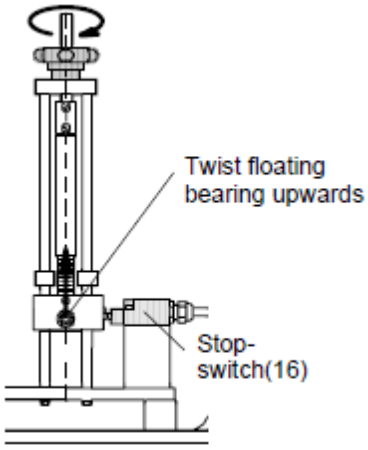

Once safe functioning of all components has been established, the experiments can begin.

Performing the experiment

Insert the test bar

- Relieve the load device using the hand wheel (the floating bearing must be at the height of the spindle)

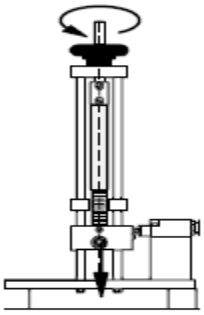

- First insert the test bar in the floating bearing of the load device

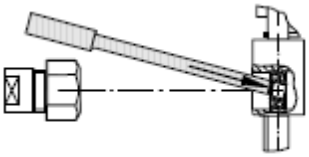

- Then insert the test bar in the collet chuck and push in as far as the end stop

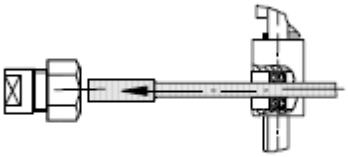

- Check concentricity of the sample by rotating the spindle by hand (correctly seated in the collet chuck, sample not deformed)
- Carefully tighten the allen key on the collet chuck and floating bearing so that the specimen is firmly placed

IMPORTANT!

Ensure that the sample is firmly seated in the collet chuck. The sample receptacle must be clean

- Mount the protective hood and lock with the knobs

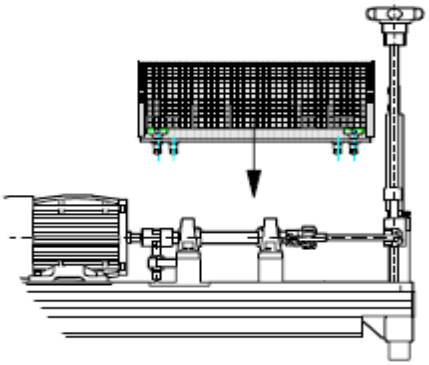

DANGER!

Never operate the revolving fatigue testing machine without the protective guard.

Parts of the sample could fly off and cause injuries when it ruptures. Rotating machine parts must be protected against accidental contact.

Start the experiment

- Switch on the motor
- Swiftly apply the required load by rotating the hand wheel. Read off the load from the computer and give the required one

IMPORTANT!

Never apply the load when the machine is idle, since there is a risk of plastic deformation and untrue running.

Bring the load to the final level as quickly as possible, because the sample is already under an alternating load but the load cycles cannot yet be counted because the load is too small.

- The counter must be zero in order to begin counting

Terminate the experiment

- The motor halts automatically when the sample ruptures. Read off the number of load cycles from the counter and make a note of the number
- or manually stop the experiment after the required number of load cycles (no rupture) by stop key in the computer
- Remove the sample. Proceed in the same manner as when inserting the test bar.

DANGER!

Risk of burns! The sample may be very hot immediately after the experiment.

ADDIS ABABA UNIVERSITY

ADDIS ABABA INSTITUTE OF TECHNOLOGY

SCHOOL OF MECHANICAL AND INDUSTRIAL ENGINEERING

DECLARATION

I, the undersigned, declare that this thesis is my original work and has not been presented for any degree in any university and all the sources of materials used for the thesis have been duly acknowledged.

Ayana Gebremichael _____ _____

Name Signature Date